Chapter 3

Proton anisotropy

3.1 Introduction

At the inner edge of the radiation belts, the trapped proton fluxes are highly anisotropic due to the interaction of the particles with the Earth's atmosphere. An important part of the flux anisotropy consists of a steep pitch-angle distribution related to the atmospheric loss cone. An additional azimuthal anisotropy appears for the high-energy trapped proton fluxes. This anisotropy is observable when the scale length of the proton radiation fluxes is comparable to or shorter than the size of the proton gyration radius. The azimuthal anisotropy results in an East-West asymmetry effect where the fluxes of protons coming—for a given position—from the East are higher than the fluxes of proton coming from the West.

One purpose of modelling this flux anisotropy is to deduce angular dependent proton flux spectra from standard omnidirectional flux data bases which were, until recently, the only ones available. Such a model has been developed analytically by Watts et al. (1989) which combines the Heckman and Nakano (1969) pitch-angle distribution with the Lenchek and Singer (1962) East-West asymmetry factor. The Watts et al. (1989) model has been used by the *Science Applications International Corporation* (SAIC) to evaluated radiation shielding for manned spacecraft (Armstrong et al. 1990; Appleby et al. 1992) and to analyse data from the LDEF satellite (Armstrong et al. 1992ab).

In the software tools ANISO and ANISOPOS developed in the framework of this study, the model of Watts et al. (1989) and an alternative version based on the Badhwar and Konradi (1990) pitch-angle distribution have been implemented. The purpose of both programmes is to provide angular dependent proton flux spectra starting from the standard omnidirectional flux model AP-8.

Since unidirectional trapped proton flux data bases are now available, our second objective is to build directional models of the radiation belt directly from these data bases. To this end, a generalised anisotropy model for the LEO radiation environment is introduced.

The Lenchek and Singer (1962) East-West asymmetry factor, the Heckman and Nakano (1969) pitch-angle distribution, and consequently the anisotropy model of Watts et al. (1989),

are based on the assumption that, at low altitude, the energetic proton flux is directly controlled by the density distribution of the Earth's atmosphere over a particle drift shell (Yoshida et al. 1960; Haerendel 1962). The anisotropy model of Watts et al. (1989) depends explicitely on the local value of the magnetic dip angle and of the atmospheric scale height. A trapped radiation belt model based on this type of description of the anisotropy will probably poorly satisfy the contraints imposed on the angular flux distribution by Liouville's theorem (Roederer 1970; Hess 1968), which links the unidirectional particle fluxes observed at two different geographic position located on a same magnetic drift shell. Such a link introduces a compulsive constraint on all models depending on local values.

In order to obtain a more general description of the trapped proton anisotropy, we introduce an alternatieve approach based only on the use of a coordinate system attached to the magnetic field lines. It results in a model which does not include parameters depending explicitly on the geographic location where the model is evaluated. This kind of approach is not original. It corresponds to the use of action variables, i.e. the adiabatic invariants μ, J and Φ (Schulz and Lanzerotti 1974).

This study has been fully reported in Technical Note 6 and Technical Note 6 Part II, which are outputs of WP.2.2 and WP.2.3R.

3.2 Conventional trapped proton anisotropy models

After defining the notations used in the following paragraphs, the pitch-angle distribution models and the effect of the finite gyroradius length will be reviewed. Afterwards, their combination will be analysed and improvements will be proposed. Special attention will be drawn to the atmospheric scale height determination and to the Armstrong et al. (1990) models VF1MIN and VF1MAX. A trapped proton anisotropy model based on the Badhwar & Konradi (1990) pitch angle distribution will also be investigated.

3.2.1 Notations

In this section, we will introduce geometric planes and direction vectors defined at the point of observation. These planes and vectors and their relative orientation are shown in Fig. 3.1. In this figure, the point of observation is located at the origin of the coordinate system. The local horizontal plane is represented, as well as the local vertical plane which contains the magnetic field line passing through the point of observation, and the plane perpendicular to the magnetic field line (mirror plane). The vector $\bar{D}$ represents an arbitrary direction which could be the look or viewing direction of a detector.

In a spherical geocentric coordinate system, the position of observation is characterized by the vector $R\,\bar{1}_R$ where R is the distance from the Earth's centre ($\bar{1}_R$ is the unit vector in the zenith direction). The altitude is given by $h = R - R_{\mathrm{E}}$, R_{E} being the Earth's radius. At this location, the geomagnetic field vector is denoted by $B\,\bar{1}_B$. In the northern hemisphere,

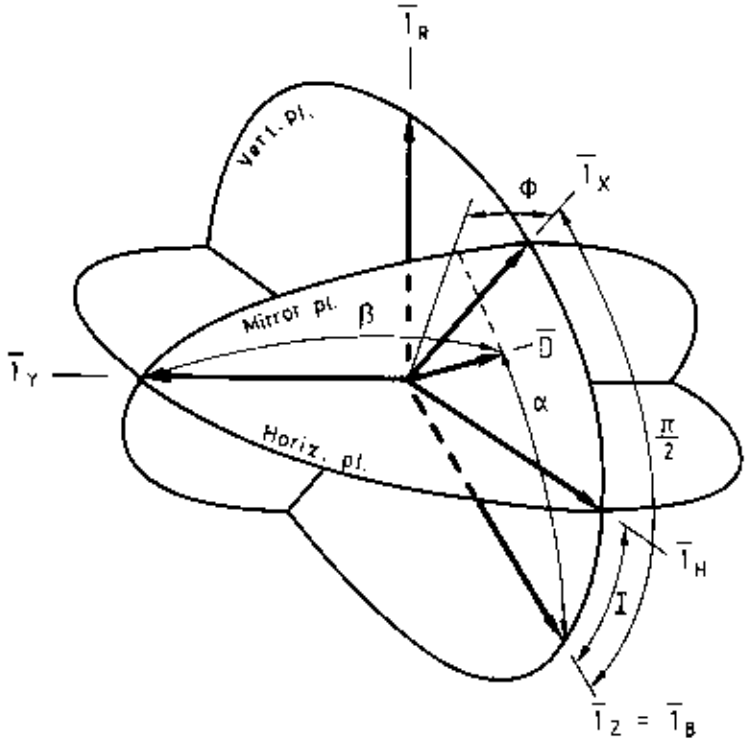

Figure 3.1. Representation of the coordinate system used in trapped proton anisotropy theory (see text)

the magnetic field vector points down to the Earth while in the southern hemisphere, it points upward away from the Earth.

A useful coordinate system is introduced with the z-axis along the magnetic field ($\bar{1}_z = \bar{1}_B$), the y-axis along the magnetic East direction ($\bar{1}_y \propto \bar{1}_B \times \bar{1}_R$) and the x-axis perpendicular to the magnetic vector in the vertical plane [$\bar{1}_x \propto (\bar{1}_B \times \bar{1}_R) \times \bar{1}_B$]. The magnetic dip angle I, i.e. the angle between the magnetic field and the horizontal plane, is defined by $\cos I = \bar{1}_H \cdot \bar{1}_B$, where $\bar{1}_H = \bar{1}_R \times \bar{1}_y$ is the intersection of the horizontal plane and the vertical plane.

In a dipole magnetic field, the position of observation is also characterized by McIlwain's (1961) magnetic shell parameter L, the magnetic latitude λ and the magnetic longitude φ. The magnetic dip angle is related to λ by

$$2 \tan \lambda \;\; = \;\; \tan I \, . \tag{3.1}$$

A vector $\bar{D}$ is specified in the coordinate system ($\bar{1}_x, \bar{1}_y, \bar{1}_z$) by a polar angle α and an azimuthal angle ϕ. An angle β is also introduced which measures the deviation from the magnetic East direction ($\cos \beta = \bar{D} \cdot \bar{1}_y = \sin \alpha \sin \phi$).

The gyroradius of a charged particle with velocity parallel to $\bar{D}$, a charge q, a mass m_0 and kinetic energy E, is given by:

$$r_{\rm g} = \frac{r_{\rm gm}}{\sin \alpha} = \tilde{r}_{\rm g} \sin \alpha \tag{3.2}$$

(Hess 1968, Walt 1994), where $r_{\rm gm}$ is the gyroradius at the mirror point of the particle, and where

$$\widetilde{r}_{\rm g} = \frac{p}{qB} = \frac{\sqrt{E^2 + 2m_0c^2E}}{qcB} \tag{3.3}$$

is the gyroradius of a particle mirroring at the position of observation where the magnetic field intensity is equal to B, and p is the relativistic momentum of the particle.

On the field line passing through the position of observation, the magnetic dip angle, the magnetic field intensity and the altitude of the mirror point are respectively $I_{\rm m}$, $B_{\rm m}$ and $h_{\rm m}$. For particles close to their mirror points at the position of observation[1], it is convenient to introduce the deviation from a 90° pitch-angle: $\theta = \pi/2 - \alpha$.

3.2.1.1 Unidirectional flux

The integral unidirectional flux J is defined as

$$J(E, \bar{D}) = \int_E^\infty j(E', \bar{D})\,{\rm d}E'\,. \tag{3.4}$$

where $j(E, \bar{D})$ is the unidirectional and differential flux of protons of energy E in the direction $\bar{D}$. Without loosing generality the differential flux can be expressed as

$$j(E, \bar{D}) = j_0(E)\ \left[\frac{1}{C}\, f(E, \theta)\, g(E, \theta, \phi)\right] \tag{3.5}$$

where $j_0(E)$ is the omnidirectional differential flux defined by

$$j_0(E) = \int_{4\pi} j(E, \bar{D})\,{\rm d}\Omega \tag{3.6}$$

and the second factor represents the angular dependence of the directional flux. The functions f and g are related respectively to the pitch-angle distribution and the azimuthal distribution with respect to the East-West direction. Note that f does not represent a phase-space distribution but represents a particle flux distribution. C is a normalisation factor.

3.2.2 Pitch-angle distribution

The pitch-angle distribution $f(\theta)\,{\rm d}\theta$ gives the flux of particles observed for pitch-angles between $\pi/2 - \theta -\ {\rm d}\theta$ and $\pi/2 - \theta$. The distributions of Heckman & Nakano (1969) and Badhwar & Konradi (1990) are reviewed and compared.

[1] When a particle is not close to its mirror point, it travels further along the field line down into the atmosphere and will be absorbed.

3.2.2.1 Heckman-Nakano pitch-angle distribution

The theoretical approach proposed by Heckman and Nakano (1969) assumes that the flux along a magnetic field line is inversely proportional to the atmospheric density at the mirror point location. This assumption is based on observations of the Explorer I satellite. In a large range of the Explorer I measurements, the radiation flux increases exponentially with the altitude (Yoshida et al. 1960). Considering as a first approximation that the atmospheric density varies as $\rho \propto \exp(-h/H)$, these observations support the assumption that the radiation flux is inversely proportional to the atmospheric density. This assumption was widely adopted [e.g. Haerendel (1962), Lenchek & Singer (1962)].

Heckman and Nakano (1969) expressed the angular distribution $f(\theta)\,\mathrm{d}\theta$ as the product of the probability P_1 that the particle has a pitch-angle between θ and $\theta + \mathrm{d}\theta$ and the probability P_2 that the particle is observed in a field line segment Δx. The probability P_1 is given by

$$P_1(\theta, \theta + \mathrm{d}\theta) \propto \frac{1}{\rho(h_\mathrm{m})}\,\mathrm{d}\ell\,, \tag{3.7}$$

where the pitch-angle range $[\theta, \theta + \mathrm{d}\theta]$ corresponds to a range $[\ell, \ell + \mathrm{d}\ell]$ of the mirror-point locations along the field line. The distance ℓ and the mirror-point altitude are approximatively related by $h_\mathrm{m} = h - \ell \sin I$.

The second probability P_2 takes into account the time $\Delta x / v_\parallel$ spent by the particle in the segment Δx (where $v_\parallel$ is the particle velocity along the field line) and τ_b the bounce period of the particle:

$$P_2 \propto \frac{\Delta x}{v_\parallel}\frac{1}{\tau_\mathrm{b}} \propto \sin^{-1}\theta\,. \tag{3.8}$$

Heckman and Nakano (1969) used a dipole field to obtain the relation between $\mathrm{d}\ell$ and $\mathrm{d}\theta$:

$$\mathrm{d}\ell = \frac{4}{3}R\left[\cos I(2+\cos^2 I_\mathrm{m})\tan I_\mathrm{m}\right]^{-1}\tan\theta\,\mathrm{d}\theta\,. \tag{3.9}$$

In a small-angle approximation, $\tan\theta = \theta$, $\sin\theta = \theta$, $I = I_\mathrm{m}$, the integration of Eq. (3.9) gives

$$\ell = \frac{2}{3}R\left[(2+\cos^2 I)\sin I\right]^{-1}\theta^2\,. \tag{3.10}$$

In an exponential atmosphere, the pitch-angle distribution $f_\mathrm{HN}(\theta)\,\mathrm{d}\theta = P_1 P_2$ is given by

$$f_\mathrm{HN}(\theta)\,\mathrm{d}\theta \propto \frac{\mathrm{d}\theta}{\exp(-h_\mathrm{m}/H)} \propto \exp(\frac{-\theta^2}{2\sigma^2})\,\mathrm{d}\theta \tag{3.11}$$

where the square of the standard deviation is defined by

$$\sigma^2 = \frac{3}{4}\frac{H}{R}(2+\cos^2 I) \tag{3.12}$$

and H is the atmospheric scale height. The Heckman-Nakano expression for the pitch-angle distribution has the advantage to be easy to use, but on the other hand, $f_\mathrm{HN}(\theta)$ is only valid for

small values of θ, and it doesn't take into account the non-dipolar terms of the geomagnetic field.

Equation (3.12) shows that the Heckman-Nakano pitch-angle distribution does not depend on the atmospheric density but depends on the density gradient, i.e. the density scale height. When the atmospheric scale height is small, the pitch-angle distribution becomes narrow when approaching $\theta = 0$. When the atmospheric scale height is larger, the pitch-angle distribution will spread and the small-angle approximation may no longer be valid. Note also that there is no true loss cone in the Heckman-Nakano formulation of the pitch-angle distribution.

3.2.2.2 Badhwar-Konradi pitch-angle distribution

Empirical pitch-angle distributions have been proposed (e.g. Valot & Engelmann 1973, Badhwar & Konradi 1990) and are characterised by the use of a loss cone angle $\alpha_{\rm L}$. The Badhwar-Konradi distribution is given by

$$f_{\rm BK}(\theta) = \begin{cases} \xi \exp(-b\xi) & |\theta| < \pi/2 - \alpha_{\rm L} \\ 0 & |\theta| > \pi/2 - \alpha_{\rm L} \end{cases} \tag{3.13}$$

where $\xi = (\cos\theta - \sin\alpha_{\rm L})/\sqrt{B}$ and b is a shape parameter. The two parameters, $\alpha_{\rm L}$ and b, have to be fitted to experimental unidirectional flux measurements. The Badhwar-Konradi distribution is an empirical fit function: it is not based on physical grounds, e.g. a pitch-angle diffusion theory. However, it gives an excellent fit for the AP-8 MIN omnidirectional fluxes, as well as for the measurements of Fischer et al. (1977).

When particles are inside the loss cone ($|\theta| > \pi/2 - \alpha_{\rm L}$), they are precipitating into the atmosphere; these particles do not contribute to the flux intensity of trapped ions: there are no particles inside the loss cone. The parameter b controls the shape of the distribution defined by Eq. (3.13) for small values of θ.

The Badhwar-Konradi pitch-angle distribution does not depend explicitly on either the atmospheric density ρ or the atmospheric scale height H. This distribution is connected to ρ and H through the loss cone $\alpha_{\rm L}$ and the empirical shape parameter b which have to be determined on a case by case basis to fit the experimental datasets.

The loss cone $\alpha_{\rm L}$ can be related to the atmospheric cut-off field intensity $B_{\rm c}$ which is the highest magnetic field intensity $B_{\rm m}$ for which the drift shell ($B_{\rm m}, L_{\rm m}$) is populated by stably trapped particles. $B_{\rm c}$ is a function of $L_{\rm m}$ and is directly related to $\alpha_{\rm L}$ by

$$\sin\alpha_{\rm L} = \sqrt{\frac{B_{\rm m}}{B_{\rm c}}}\,. \tag{3.14}$$

The magnetic cut-off $B_{\rm c}$ and the loss cone angle $\alpha_{\rm L0}$, obtained from

$$\sin\alpha_{\rm L0} = (B_{\rm c}/B_0)^{-1/2}\,, \tag{3.15}$$

are different for different magnetic field and atmospheric models. The parameters $B_{\rm c}$ and $\alpha_{\rm L}$, and their dependence on $L_{\rm m}$ must be re-evaluated for each new dataset, and are specific to the epoch of the magnetic field model used.

3.2.2.3 Comparison between Heckman-Nakano and Badhwar-Konradi distributions

The Heckman-Nakano and the Badhwar-Konradi expressions correspond to two different approaches:

- Badhwar and Konradi (1990) propose an empirical fit function applied to an experimental trapped particle dataset (e.g. AP-8 MIN), while Heckman and Nakano's (1969) approach is a theoretical one which depends on a model of the atmospheric scale height and on an assumption linking the atmospheric density to the radiation flux.
- The parameter σ of the pitch-angle distribution $f_{\rm HN}(\theta)$ is defined locally in geographic coordinates, while the $f_{\rm BK}(\theta)$ parameters $\alpha_{\rm L}$ and b only depend on E and $L_{\rm m}$, as a consequence of Liouville's theorem (see Sect. 3.2.4.3).

The Badhwar-Konradi parameters $\alpha_{\rm L}$ and b [Eq. (3.13)] have been obtained from a fitting procedure (Heynderickx & Lemaire 1993) of an unidirectional version of the AP-8 MIN model where the value of L is determined using the Jensen and Cain (1962) geomagnetic field model and the energy is set to E =20 MeV (the parameters $\alpha_{\rm L}$ and b vary slightly with energy).

To evaluate the Heckman-Nakano parameter σ [Eq. (3.12)], the atmospheric density scale height given by

$$H = 33.4\,{\rm km} \times \exp\left(\frac{R - 6371.2\,{\rm km}}{383\,{\rm km}}\right) \tag{3.16}$$

is used. Equation (3.16) corresponds to the atmospheric scale height used by Colborn et al. (1990) when applying the Watts et al. (1989) model for solar minimum.

In Fig. 3.2, the pitch-angle distributions $f_{\rm HN}$ and $f_{\rm BK}$ are compared at two geographic locations: (394.3 km, 25.7°S, 51.0°W) and (720.8 km, 7.9°S, 15.0°W), i.e. two mirror points on the same drift shell defined by $L = 1.24$ and $B_{\rm m} = 0.2$. At 394.3 and 720.8 km altitude, the atmospheric scale height of Eq. (3.16) is equal to 93.5 and 219.3 km, respectively. For the purpose of comparison, the parameters b and $\alpha_{0\rm c}$ of the Badhwar & Konradi (1990) function have been fitted to the SAMPEX countrates presented later in Sect. 3.3.4 (see Fig. 3.11). For both distributions, the unidirectional flux has been normalized to 1 at α =90°.

The Badhwar-Konradi pitch-angle distribution is steeper than the Heckman-Nakano distribution: beyond the local pitch-angle $\alpha_{\rm L}$, $f_{\rm BK}(\alpha)$ =0, whereas $f_{\rm HN}(\alpha)$ does not vanish within the loss cone. Remember, however, that for pitch-angles faraway from 90°, Heckman and Nakano's small-angle approximation is no more valid.

Since the Badhwar & Konradi (1990) function depends only on E and L, the $f_{\rm BK}$ pitch-angle distribution is identical at both locations. On the other hand, the variation of the ratio H/R from $1/72$ to $1/32$ between the two locations implies an important change of the Heckman & Nakano (1969) pitch-angle distribution. According to Liouville's theorem (see Sect. 3.2.4.3) the pitch-angle distributions at the mirror point must be the same as at any mirror point on the same drift shell, including the lowest-altitude mirror point. Therefore, models based on the $f_{\rm HN}$ function have to be restricted to a region of space where the ratio H/R does not vary.

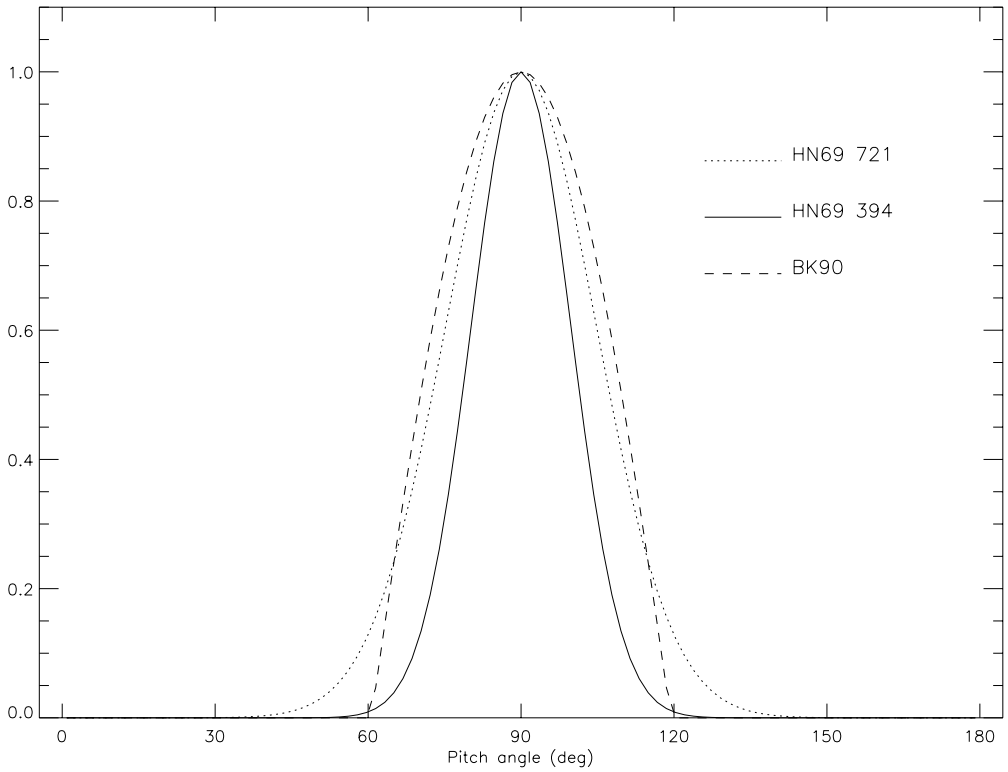

Figure 3.2. Comparison of the Heckman & Nakano (1969) and Badhwar & Konradi (1990) pitch angle distributions at $L = 1.24$ and $B_{\rm m} = 0.2$. The dotted and solid lines correspond to the Heckman & Nakano (1969) distribution evaluated at an altitude of 720.8 and 394.3 km, respectively. The dashed line corresponds to the Badhwar & Konradi (1990) distribution, whatever the altitude. Note that the normalisation is such that $f(\pi/2) = 1$.

In conclusion, Heckman-Nakano's and Badhwar-Konradi's pitch-angle distributions produce qualitatively similar results. However, the Heckman and Nakano (1969) results deviate from the expected result at higher altitude. The Badhwar and Konradi approximation is adiabatically invariant, since it depends only on the (B, L) coordinate system which are adiabatic invariants in a static magnetic field; this guarantees a satisfactory pitch-angle distribution at all altitudes.

3.2.3 Lenchek-Singer East-West asymmetry model

The Lenchek & Singer (1962) model is the first and, to our konwledge, the only one, describing the azimuthal distribution of the trapped particle fluxes at low altitude where East-West effects become important.

As depicted by Lenchek and Singer (1962), for a given point of observation, protons coming from the West have their guiding centres above the point of observation, while those coming from the East have their guiding centres below this point. Therefore, during their drift, protons

coming from the West will experience averaged atmospheric densities smaller than those with the same pitch angle but coming from the East. This East-West asymmetry is observable when the gyroradii of the trapped protons become comparable with the atmospheric scale heights, H.

For a proton at an altitude h with a velocity in the direction $\bar{D}$ (e.g. the axis of the detector), the altitude of the local guiding centre is given by $h + r_{\rm g} \cos I \cos \beta$. Let $h_{\rm m}$ be its mirror point altitude in the guiding centre approximation, i.e. on the field line passing through the point of observation. When the gyroradius is not small compared to the atmospheric scale height, its mirror point altitude will be given by $h_{\rm m} + r_{\rm gm} \cos I_{\rm m} \cos \beta_{\rm m}$. Assuming that the atmospheric density decreases exponentially with a scale height H and that the flux is inversely proportional to the atmospheric density at the mirror point (see Sect. 3.2.2.1), the omnidirectional flux at h and $h_{\rm m}$ has to be corrected by a factor proportional to

$$\frac{\exp\left(-\dfrac{h_{\rm m}}{H}\right)}{\exp\left(-\dfrac{h_{\rm m} + r_{\rm gm} \cos I_{\rm m} \cos \beta_{\rm m}}{H}\right)} = \exp\left(\frac{r_{\rm gm} \cos I_{\rm m} \cos \beta_{\rm m}}{H}\right) . \tag{3.17}$$

Note that this correction depends on the local magnetic field configuration in the neighbourhood of the mirror point. Therefore, the correction factor may be different for all mirror points of a given drift shell $(B_{\rm m}, L_{\rm m})$.

In order to avoid field line tracing, the correction factor may be approximated by

$$g_{\rm LS}(\theta, \phi) = \exp\left(\frac{\widetilde{r}_{\rm g} \cos I \sin \alpha \sin \phi}{H}\right) \tag{3.18}$$

when the pitch-angle is near 90°, $I_{\rm m} \simeq I$, $\beta_{\rm m} \simeq \beta$, $r_{\rm gm} \simeq \widetilde{r}_{\rm g}$, where $\widetilde{r}_{\rm g}$, the gyroradius of particles mirroring at the point of observation, is given by Eq. (3.3). Expression (3.18) has the advantage to be easy to use and to outline the dependence on the pitch-angle α and on the azimuthal direction ϕ.

Of course, when the gyroradius of a trapped ion becomes larger than the density scale height this first order approximation should become questionable. But so far no other alternative and more general theory has been proposed.

3.2.4 Combination of the angular distributions

In the previous sections, models for the pitch-angle and azimuthal distributions have been reviewed. In order to obtain the total angular distribution of the proton or heavier ion fluxes the pitch-angle distribution and the East-West asymmetry distribution must be combined and renormalized.

Let $f(E, \theta)$ be the pitch-angle distribution and $g(E, \theta, \phi)$ the distribution with respect to the East-West direction where $\theta = \pi/2 - \alpha$ is the complement of the pitch-angle, and ϕ is the azimuthal angle. The differential unidirectional flux then becomes

$$j = j_0(E)\, \frac{1}{C}\, f(E, \theta)\, g(E, \theta, \phi)\,, \tag{3.19}$$

where j_0 is the omnidirectional trapped proton flux and C is a normalisation factor. Note that this decomposition of the unidirectional flux is not restrictive. The factor C and the functions f and g have to be determined so that the omnidirectional flux computed from Eq. (3.19) is equal to $j_0(E)$, i.e.

$$\int_0^{\pi}\int_0^{2\pi} j \; \mathrm{d}\phi \, \mathrm{dcos}\, \alpha = j_0(E)\,. \tag{3.20}$$

There are different methods to satisfy this normalisation condition. Each method leads to a different expression of the unidirectional flux j, but each expression will provide the same omnidirectional flux j_0. Below, we restrict our description to the two most commonly used methods.

3.2.4.1 Global normalisation

The first method of normalisation is to define the factor C in Eq. (3.19) as

$$C = \int_0^{\pi}\int_0^{2\pi} f(E, \tfrac{\pi}{2} - \alpha) g(E, \tfrac{\pi}{2} - \alpha, \phi) \, \mathrm{d}\phi \, \mathrm{dcos}\, \alpha\,. \tag{3.21}$$

In this case, the factor C is a constant, i.e. it depends neither on α nor on ϕ. For instance, when g_{LS} is used to describe the East-West asymmetry distribution, the integration over ϕ is analytical and the factor C is given by Kern (1989):

$$C_{\mathrm{G}} = 2\pi \int_0^{\pi} f(E, \tfrac{\pi}{2} - \alpha) \, \mathrm{I}_0\!\left(\frac{\widetilde{r}_{\mathrm{g}} \cos I \sin \alpha}{H}\right) \mathrm{dcos}\, \alpha\,, \tag{3.22}$$

where I_0 is the zero order modified Bessel function (Abramowitz and Stegun, 1964).

3.2.4.2 Separate normalisation

A second method of normalisation consists of normalizing separately the two functions f and g:

$$C_f = \int_0^{\pi} f(\tfrac{\pi}{2} - \alpha) \, \mathrm{dcos}\, \alpha \tag{3.23}$$

and

$$C_g = \int_0^{2\pi} g(\tfrac{\pi}{2} - \alpha, \phi) \, \mathrm{d}\phi\,. \tag{3.24}$$

In this case, the total normalisation factor is given by

$$C = C_f \, C_g\,. \tag{3.25}$$

Note that the total normalisation factor C now depends on the angle α. For instance, when g_{LS} is used to describe the East-West asymmetry, the factor C will be given by

$$C_{\mathrm{S}} = 2\pi \, \mathrm{I}_0\!\left(\frac{\widetilde{r}_{\mathrm{g}} \cos I \sin \alpha}{H}\right) \int_0^{\pi} f(\tfrac{\pi}{2} - \alpha) \, \mathrm{dcos}\, \alpha\,. \tag{3.26}$$

Obviously, the expressions (3.22) and (3.26) are different. These two expressions will lead to two different expressions for the unidirectional flux, but both will provide the same omnidirectional flux $j_0(E)$.

Therefore, a trapped proton anisotropy model is determined by a selection of an omnidirectional flux j_0, a pitch-angle distribution f, an azimuthal distribution g, and by the choice of the normalisation method: Eqs. (3.22) or (3.26).

3.2.4.3 Liouville's theorem

As explained previously [see Eq. (3.19)], to create an anisotropy model, a pitch-angle distribution as well as a East-West asymmetry angular distribution must be selected or determined experimentally. Until a more comprehensive physical model is available, different criteria (e.g. the ease of use, the accuracy, etc.) will be used to select the appropriate distributions. In this section, we will study the constraint on the angular distribution functions f and g resulting from the application of the Liouville's theorem. This constraint affects the parameters on which the angular distributions depend.

In a stationary geomagnetic field and when magnetic field lines are electric equipotentials, the magnetic field intensity $B_{\rm m}$ at the mirror point and the McIlwain (1961) parameter $L_{\rm m}$ fully characterize a drift shell of trapped particles, i.e. the whole shell of guiding center field lines. Consider now unidirectional particle fluxes observed at two different locations $\bar{r}$ and $\bar{q}$ on a same drift shell. In the absence of Coulomb or wave-particle interactions, according to Liouville's theorem for trapped particles (Roederer 1970, Hess 1968), the fluxes are related by

$$\int_0^{2\pi} \frac{j(\bar{r},\alpha_r,\phi_r)}{E}\,\mathrm{d}\phi_r = \int_0^{2\pi} \frac{j(\bar{q},\alpha_q,\phi_q)}{E}\,\mathrm{d}\phi_q\,. \tag{3.27}$$

In a stationary magnetic field, when the flux is assumed to be gyrotropic, Expression (3.27) reduces to $j(\bar{r},\alpha_r) = j(\bar{q},\alpha_q)$. The pitch-angles are determined by the conservation of the first adiabatic invariant, i.e. the magnetic moment:

$$\frac{\sin^2\alpha_r}{B(\bar{r})} = \frac{\sin^2\alpha_q}{B(\bar{q})}\,. \tag{3.28}$$

At two points where the magnetic field intensities are equal, $\alpha_r = \alpha_q$ and

$$f(\bar{r},\theta)\int_0^{2\pi} g(\bar{r},\theta,\phi_r)\,\mathrm{d}\phi_r = f(\bar{q},\theta)\int_0^{2\pi} g(\bar{q},\theta,\phi_q)\,\mathrm{d}\phi_q\,. \tag{3.29}$$

This relation is the basic constraint on the angular flux distribution imposed by Liouville's theorem.

When the flux is gyrotropic (i.e. independent of ϕ), the constraint (3.29) shows that the pitch-angle distribution observed at conjugate points [i.e. with the same (B, L) coordinates] must be equal. This condition is satisfied by a pitch-angle distribution like $f_{\rm BK}$ given by Eq. (3.13), where the controlling parameters $\alpha_{\rm L}$ and b depend on E and $L_{\rm m}$. On the other hand, the pitch-angle distribution $f_{\rm HN}$ does not satisfied Condition (3.29), since the controlling parameters h, H

and I of this pitch-angle distribution are evaluated at the point of observation. One way to meet Condition (3.29) with the Heckman-Nakano pitch-angle distribution would be to use effective parameters depending on coordinates such as $B_{\rm m}$ or $L_{\rm m}$, which both are adiabatic invariants in a static magnetic field. For instance, an effective scale height $H_{\rho'}$ may be defined as the scale height of the averaged atmospheric density over a drift shell.

When the azimuthal distribution due to the East-West effect is important, due to Constraint (3.29), the functions f and g are not independent from one another. A common practice is to simply meet separately the two following conditions:

$$f(\bar{r},\theta) = f(\bar{q},\theta) \tag{3.30}$$

and

$$\int_0^{2\pi} g(\bar{r},\theta,\phi_r)\,\mathrm{d}\phi_r = \int_0^{2\pi} g(\bar{q},\theta,\phi_q)\,\mathrm{d}\phi_q\,. \tag{3.31}$$

For instance, to satisfy Condition (3.31) with the Lenchek-Singer distribution [see Eq. (3.18)], one has to use an effective atmospheric scale height averaged over the whole drift shell. Furthermore, one has to use either a separate normalisation [see Sect. 3.2.4.2], or to restrict the application of the model to a simple centered dipole magnetic field.

In short, Liouville's theorem, which links particle flux observed at different locations on a drift shell, imposes a drastic condition [Eq. (3.29)] to the experimental or theoretical angular distribution for trapped proton directional flux models. When the separate normalisation [Eqs. (3.23) and (3.24)] is used, this criterion is reduced to Eq. (3.30). Therefore, parameters like ($B_{\rm m}$, $L_{\rm m}$, $\alpha_{\rm L}$, $H_{\rho'}$, $h_{\widetilde{\rm m}}$, ...) averaged over drift shells have to be preferred to local parameters like h, H, I to determine pitch angle distributions.

3.2.5 Armstrong and Watts models

Armstrong et al. (1990) applied the model for angular distribution developed by Watts et al. (1989) for the AP-8 MIN and MAX model to evaluate differential energy spectra of trapped proton unidirectional fluxes at low altitude. The assumptions on which this model is based have been discussed in another section. The energy spectra presented by these authors were averaged over circular orbits with a 28.5° inclination and an altitude ranging from 300 to 500 km. To analyse the radiation environment of the Space Station, Armstrong et al. (1990) converted the energy spectra to Si and Blood Forming Organs (BFO) doses using Burrell's (1964) one-dimension proton transport code. To compare their prediction with data from the Long Duration Exposure Facility (LDEF), Armstrong et al. (1992b) also developed a three-dimensional transport calculation based on the High-Energy Transport Code (HETC) code (Armstrong & Chandler 1972). The comparison showed that AP-8 underestimates the LDEF data by about a factor of 2 and that the Watts et al. (1989) model produces weaker anisotropies than those observed. This latter discrepancy can be attributed to the inappropriate atmospheric scale height used in Armstrong et al.'s (1990) calculation.

In this section, we describe the trapped proton anisotropy models labelled VF1MIN and VF1MAX by Colborn et al. (1990). VF1 stands for Vector Fluxes, version 1. The VF1MIN

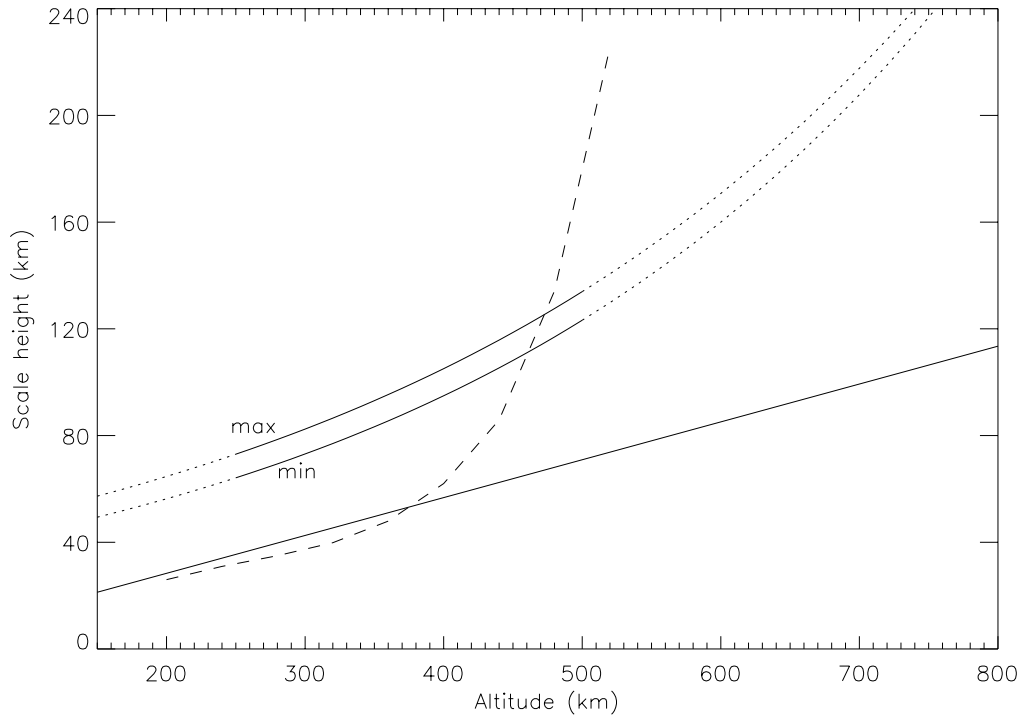

Figure 3.3. Comparison between different scale heights. The dotted-partly-solid lines represent effective scale heights $H^{\min}$ and $H^{\max}$ used by Armstrong et al. (1990) and given in Eqs. (3.32) and (3.33). The solid line is the scale height obtained from Allen's (1985) atmosphere model. The dashed line correspond to the stopping-power scale height as a function of $h_{\widetilde{m}}$ (Heckman & Brady 1966).

and VF1MAX models correspond to solar minimum and solar maximum. In these models, conversion factor, to transform omnidirectional flux into unidirectional flux, is given by

$$W_{\rm VF}(E,\alpha,\phi) = \frac{\exp\left(-\dfrac{(\pi/2-\alpha)^2}{2\sigma^2}\right)}{\sin\alpha\sqrt{2\pi}\sigma{\rm erf}\left(\dfrac{\pi}{\sqrt{8}\sigma}\right)} \frac{\exp\left(\dfrac{r_{\rm g}\cos I\sin\phi}{H}\right)}{2\pi{\rm I}_0(r_{\rm g}\cos I/H)} \tag{3.32}$$

where ${\rm I}_0$ is the modified Bessel function. Note that Eq. (3.32) is deduced from a separated normalisation where $f_{\rm HN}$ is normalized with respect to α instead of $\cos\alpha$. The omnidirectional spectra $j_0(E)$ at solar minimum and solar maximum are taken from the AP-8 MIN and MAX models respectively. Colborn et al. (1990) have used the atmospheric scale height H obtained from the Johnson and Smith (1985) atmospheric model: H is an increasing function of the altitude which has been approximated for solar minimum and maximum by

$$H^{\min} = 33.4{\rm km}\times\exp\left(\frac{h}{383{\rm km}}\right), \tag{3.33}$$

$$H^{\max} = 39.8{\rm km}\times\exp\left(\frac{h}{412{\rm km}}\right). \tag{3.34}$$

Expressions (3.33) and (3.34) are assumed to be valid in an altitude range between 250 and 500 km. In this study, we have reconstructed the models VF1MIN and VF1MAX from Eqs. (3.32)–(3.34) where the modified Bessel function is evaluated by the expansion series

$$C_{g\mathrm{W}} = 2\pi \sum_{k=0}^{\infty} \frac{1}{k!^2} \left(\frac{r_g \cos I \sin \alpha}{2H} \right)^{2k} \tag{3.35}$$

which converges rapidly (Evans & Daly 1989).

In Fig. 3.3, Colborn et al. (1990) scale heights are compared to the atmospheric scale height $H(h)$ based on Allen's (1985) table of atmospheric densities and Heckman & Brady's (1966) effective scale height $H_{\Delta E}$ based on the energy loss by a particle along its trajectory. The atmospheric scale height $H(h)$ (full solid line) and Colborn et al. (1990) effective scale heights $H^{\min}$ and $H^{\max}$ (dotted-partly-solid lines) are functions of the altitude h. The Heckman & Brady (1966) effective scale height $H_{\Delta E}$ (dashed line) has been determined for a set of drift shells $(B_{\mathrm{m}}, L_{\mathrm{m}})$ where L_{m} is fixed at 1.38 and where B_{m} varies from 0.2043 to 0.2355 gauss. The effective energy loss scale height $H_{\Delta E}$ is a function of the lowest mirror point altitude $h_{\widetilde{\mathrm{m}}}$.

The shapes of the Colborn et al. (1990) scale heights are similar for solar minimum and solar maximum. The difference between $H^{\min}$ and $H^{\max}$ does not exceed 11 km in the altitude range 250–500 km. In that altitude range, $H^{\min}$ and $H^{\max}$ are about 45 km larger than Allen's (1985) atmospheric scale height. Additional atmospheric models can, of course, also be used to determine this latter local density scale height. It can be seen that the altitude distribution of the effective scale height $H_{\Delta E}$ is quite different from all others. Below 350 km, $H_{\Delta E}$ is almost equal to the local atmospheric scale height of Allen's (1985) model. At these altitudes, the main constituents of the atmosphere are N_2, O_2, and O which have almost the same ratio A/Z. Therefore the rate of energy loss is proportional to the atmospheric density. Above 350 km, Heckman and Brady's (1966) effective scale height increases very sharply, indeed the abundance of He and H is increasing about this height. Consequently, the ionization energy losses are no longer proportional to the total atmospheric density.

Note that $H_{\Delta E}$ is a function of B_{m} and L_{m}; it is not a function of the altitude of the point of observation. For instance, when an observer is located at different positions corresponding to B_{m} =0.2230 gauss and L_{m} =1.38, the altitude of his actual position may vary from 326 to 1,670 km but the effective scale height $H_{\Delta E}$ will be constant and equal to 41 km. In contrast, according to Expr. (3.34), at 326 km the scale height $H^{\max}$ will be about 88 km while at 1,670 km it will be larger than 2,000 km!

Since Armstrong et al. (1990) restrict their model to the altitude range between 250 and 500 km, trapped protons are only observed in the South Atlantic Anomaly, where the mirror points are the lowest ones. When the observer is not near the position of a lowest mirror point, the drift shell generally hits the Earth's surface in the vicinity of the South Atlantic Anomaly. Therefore, when the Armstrong et al. (1990) model is supposed to become inadequate, the radiation flux of protons is negligible. However, their model provides reasonable values of the scale height of pitch-angles close to 90°, i.e. where the directional proton flux is maximum.

Table 3.1. Values of the parameters relative to BK-MIN and BK-MAX trapped proton flux anisotropy models

Model	H	p_1	p_2	p_3	p_4
BK-MIN	100.0	−0.032392	0.039836	0.13164	−8.8674
BK-MAX	100.0	−0.031690	0.039119	0.09294	−6.1651

3.2.6 BK-MIN and BK-MAX models

We define also two very simple models based on the Badhwar and Konradi (1990) pitch-angle distribution. The models will be called BK-MIN and BK-MAX, respectively for solar minimum and solar maximum conditions.

In these models, the anisotropy conversion factor to transform omnidirectional flux into unidirectional flux, is deduced from Eqs. (3.13) and (3.18) with a separate normalisation (see Sect. 3.2.4.2). When $\alpha_{\rm L} < \alpha < \pi - \alpha_{\rm L}$, it is given by

$$W_{\rm BK}(E,\alpha,\phi) = \frac{\xi(\alpha)\exp(-b\xi(\alpha))}{2\int_{\alpha_{\rm L}}^{\pi/2}\sin\alpha'\xi(\alpha')\mathrm{d}\alpha'}\,\frac{\exp\left(\dfrac{r_{\rm g}\cos I\sin\phi}{H}\right)}{2\pi \mathrm{I}_0(r_{\rm g}\cos I/H)}\,, \tag{3.36}$$

where $\xi(\alpha) = (\sin\alpha - \sin\alpha_{\rm L})/\sqrt{B}$. When $\alpha \leq \alpha_{\rm L}$, the conversion factor is given by $W_{\rm BK}(E,\alpha,\phi) = 0$. The integral in Eq. (3.36) is evaluated numerically by a Gauss-Legendre quadrature. The loss-cone angle $\alpha_{\rm L}$ is related to the equatorial loss-cone angle $\alpha_{\rm L0}$ by the conservation of the magnetic moment [see Eq. (3.28)]:

$$\sin\alpha_{\rm L} = \sqrt{\frac{B}{B_0}}\sin\alpha_{\rm L0} \tag{3.37}$$

When, at the location of observation, B is greater than $B_0/\sin^2\alpha_{\rm L0}$, the trapped protons are absorbed by the atmosphere and the proton flux is set equal to zero.

The equatorial loss-cone pitch angle $\alpha_{\rm L0}$, the slope parameter b and scale height H are functions of the drift shell parameter L. For the sake of simplicity, H is set to a constant value and the parameters $\alpha_{\rm L0}$ and b are defined as functions of L.

The parameters $\alpha_{\rm L0}$ and b are obtained from the fit of the distribution $f_{\rm BK}$ to the AP-8 unidirectional fluxes of 20 MeV trapped protons. The parameters are closely approximated by the expressions:

$$\alpha_{\rm L0}^{-1} = p_1 + p_2\,L \tag{3.38}$$

and

$$b^{-1} = p_3 + p_4\ln L\,, \tag{3.39}$$

where $\alpha_{\rm L0}$ is expressed in degrees and b in gauss$^{\frac{1}{2}}$. The values of the scale heights and of the different parameters p_1, p_2, p_3 and p_4 are given in Table 3.1 for solar minimum and maximum conditions. The parameters p_1, p_2, p_3 and p_4 were evaluated for 20 MeV protons; their values vary slightly with the proton energy.

3.3 Generalised anisotropy model

For a point of observation located at the inner edge of the radiation belts, the observed flux of energetic trapped protons is known to depend on the look direction, even for a fixed pitch angle (Watts et al. 1989). This effect is known as the East-West asymmetry (Heckman & Nakano 1963). For instance, aboard the SAMPEX spacecraft, the countrate associated to 86–120 MeV protons and observed at $L \approx 1.15$ and $B_{\rm m} \approx 0.197$ Gauss varies by a factor of 6 between the periods when the detector is looking to the East and the periods when it is looking to the West (Looper et al., 1997). This East-West effect is explained by the fact that protons viewed with the same pitch angle but in different azimuthal directions have their guiding centres on different magnetic field lines and thus belong to different drift shells, where the fluxes are rather different from each other. Consequently, to take into account that the guiding centres of the observed protons no longer correspond to the point of observation, the L value $L_{\rm GC}$ associated with the guiding centre should be used instead of the L value associated with the point of observation. This approach means that the flux maps have to be organized in (E, $B_{\rm m}$, $L_{\rm GC}$).

3.3.1 First order expansion of the perpendicular flux

The shell parameter $L_{\rm GC}$ associated to a guiding centre depends on the look direction and also on the particle energy through the Larmor radius

$$r_{\rm g} = \frac{p}{qB} \sin\alpha \tag{3.40}$$

where p and q are the momentum[2] and charge of the proton, respectively, and B, the local magnetic field intensity. Therefore, when building and using a model of the form $f(E, B_{\rm m}, L_{\rm GC})$, $L_{\rm GC}$ has to be evaluated for every look direction and for each energy covered by the instrument. As the computation of L involves an integration along a field line segment, building and using such models is very demanding of CPU time.

To avoid the evaluation of $L_{\rm GC}$ when using the $j_\perp(E, B_{\rm m}, L_{\rm GC})$ map, an alternative approach which uses an expansion to first order in L of the perpendicular flux is applied instead. With this approximation, the flux can be written as

$$\begin{aligned} f_{\rm P}(E,\alpha,\beta) &= j_\perp(E, B_{\rm m}, L_{\rm GC}) \\ &= j_\perp(E, B_{\rm m}, L) + \Delta L \times \left.\frac{\partial j_\perp}{\partial L}\right|_{E,B_{\rm m}} + O^{(2)}(\Delta L) \end{aligned} \tag{3.41}$$

where $\Delta L \equiv L_{\rm GC} - L$. The $L_{\rm GC}$ evaluation problem is now reduced to evaluating ΔL, for which we propose an analytical expression in the next section. As shown below, ΔL is in close relationship with the distance between the point of observation P and the drift shell of the observed protons. For example, when P is located in the magnetic equatorial plane of a centred dipole field, ΔL is equal to the distance between the drift shell and P.

[2]The particle momentum and energy are related by $p^2c^2 = E^2 + 2m_0c^2E$ where c is the speed of light and m_0 the rest mass of the particle. For protons, $m_0 = 1.6725\,10^{-27}$ kg.

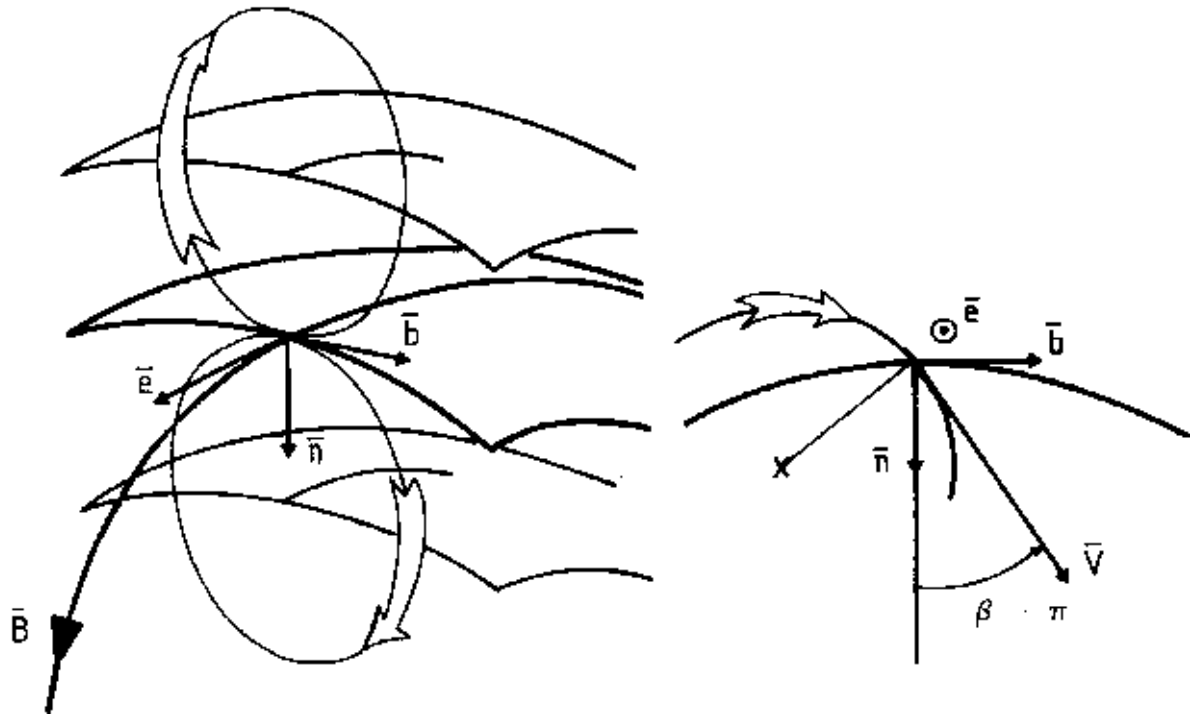

Figure 3.4. Left panel: representation of a magnetic field line segment and of three neighbouring magnetic drift shells separated by one gyroradius. The circles represent the proton gyration motions. $\mathbf{e}$, $\mathbf{n}$, And $\mathbf{b}$ are the vectors tangent, normal and bi-normal to the magnetic field line, respectively. Right panel: cut view in the plane $(\mathbf{n}, \mathbf{b})$ perpendicular to the magnetic field.

3.3.2 Natural coordinate system

To evaluate $\Delta L = L_{\rm GC} - L$, we will characterize the look direction by a pair of polar and azimuthal angles (α, β) measured in a local coordinate system attached to the local magnetic field line. Since the drift velocity of the guiding centre of a particle is perpendicular to both the magnetic field vector $\mathbf{B}$ and the perpendicular gradient $\nabla_\perp B$ (Roederer 1970), a natural coordinate system is such that

- the origin coincides with the point P of observation;
- the z-axis points in the direction $\mathbf{e}$ of the magnetic field vector;
- the x-axis points in the direction $\mathbf{n}$ of the normal to the magnetic field line;
- the y-axis points in the direction $\mathbf{b} = \mathbf{e} \times \mathbf{n}$ of the bi-normal to the magnetic field line.

The coordinate system $(\mathbf{e}, \mathbf{n}, \mathbf{b})$ is represented in the left hand panel of Fig. 3.4 where a magnetic field line and three neighbouring drift shells are shown. The typical cyclotron motion of particles attached to upper and lower drift shells are displayed also. The figure illustrates that

particles coming from the right do not belong to the same drift shell as particles coming from the left. If a gradient of particle flux exists, the flux of particles observed from both directions will differ. The right hand panel of Fig. 3.4 is a cut view in the plane $(\mathbf{n}, \mathbf{b})$ on which the azimuthal angle $\beta - \pi$ is defined.

In the coordinate system $(\mathbf{e}, \mathbf{n}, \mathbf{b})$, the magnetic field line and the drift shell passing through the point of observation P are parallel to the axis $\mathbf{e}$ and the plane $(\mathbf{n}, \mathbf{b})$, respectively. Consequently, when a proton is observed in the look direction (α, β), its pitch angle is equal to $\pi - \alpha$. Its gyration motion correponds to a clockwise circular motion in the plane $(\mathbf{n}, \mathbf{b})$ which is perpendicular to $\mathbf{B}$. Since the local guiding centre Q of the observed proton lies in both the plane $(\mathbf{n}, \mathbf{b})$ and the plane perpendicular to the look direction, the direction of Q is given by $(\pi/2, \beta + \pi/2)$. The distance between the local guiding centre and P is the Larmor radius $r_{\rm g}$ given by Eq. (3.40).

In the following, we will assume that $r_{\rm g}$ remains much smaller than the scale length of the magnetic field. Since the scale length of the magnetic field is about a third of the geocentric distance, this assumption remains valid in a large energy range. With this assumption, the magnetic field does not change significantly from P to Q and we can assume that the coordinate systems $(\mathbf{e}, \mathbf{n}, \mathbf{b})$ at these two locations are identical. The drift shell of a proton observed in the look direction (α, β) then contains Q and is parallel to the plane $(\mathbf{b}, \mathbf{e})$. The distance from P to the drift shell is given by

$$d_{\rm P}(\alpha, \beta) = r_g \cos(\beta + \pi/2) = -\frac{p}{qB} \sin\alpha \sin\beta \,. \tag{3.42}$$

One should note that protons viewed in the direction $(\alpha, \pi - \beta)$ will belong to the same drift shell as protons viewed in the direction (α, β) and that the proton fluxes in these two directions should be identical. In particular, when the azimuthal direction β is equal to 0 or π, the drift shell of the observed protons passes through the point of observation and $\Delta L = 0$.

3.3.3 Evaluation of ΔL

To establish the relationship between ΔL and the parameters such as α, β, B, L, and E, we will first connect ΔL with these parameters at the local magnetic equator[3]. Then, the parameters at the local magnetic equator will be connected to the same parameters at the current point of observation.

Since L is defined in a centred magnetic dipole by the geocentric distance of the drift shell in the equatorial plane, we can assume that ΔL is well approximated by the distance at the magnetic equator between the drift shell of the observed proton and the drift shell passing through the point of observation, i.e.

$$\Delta L \approx -d_{\rm P_0}(\alpha_0, \beta_0) \,, \tag{3.43}$$

[3]In a non-dipolar magnetic field, we define the local magnetic equator as the surface where the magnetic field intensity is minimum along magnetic field lines.

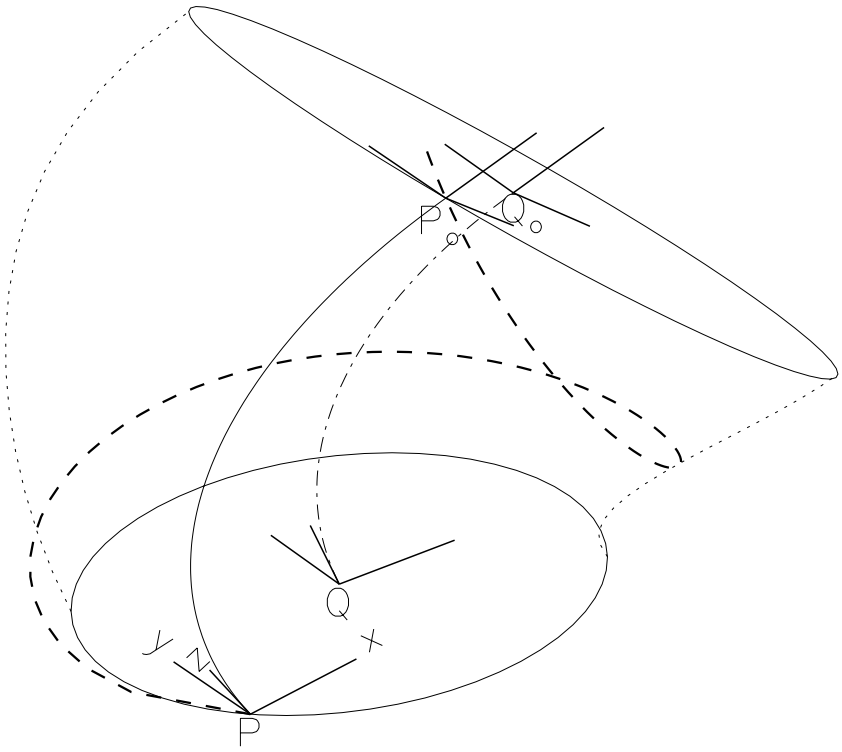

Figure 3.5. Representation of the helicoidal trajectory (dashed curve) of a particle around its guiding centre (dot-dash curve). When the particle passes through the point P ($\mathtt{P}_0$), its instantaneous guiding centre is located at Q ($\mathtt{Q}_0$). The two points P and $\mathtt{P}_0$ are located on the same magnetic field line (solid curve).

where (α_0, β_0) is the look direction of protons belonging to the same drift shell as Q but viewed from a point $\mathtt{P}_0$ in the magnetic equatorial plane which belongs to the magnetic field line passing through P. The minus sign takes into account that the distance to the drift shell is measured along the $\mathbf{n}$-axis which points in the direction of decreasing L.

The previous statements are illustrated in Fig. 3.5 where the dashed curve represents the helicoidal trajectory of a proton passing through P. Its guiding centre is represented by the dot-dash curve and includes the point Q. The magnetic field line passing through P is represented by a solid curve. The axes of the coordinate system ($\mathbf{e}$, $\mathbf{n}$, $\mathbf{b}$) are represented at both points P and Q. According to the conservation of the magnetic moment, after one, two, three, ... gyrations, the trajectory of the proton will cross again the magnetic field line passing through P. So, protons belonging to the guiding centre passing through Q can be always observed from the equatorial point $\mathtt{P}_0$ of the magnetic field line passing through P. For the sake of clarity, the helicoidal trajectory of Fig. 3.5 is passing through $\mathtt{P}_0$ after one gyration motion, which is generally not the case.

Protons belonging to the guiding centre passing through Q can be observed from both lo-

cations P and $\mathtt{P}_0$ but with different look directions: (α, β) and (α_0, β_0), respectively. The relationship between the polar angles α and α_0 is directly given by the conservation of the first adiabatic invariant:

$$\frac{\sin^2 \alpha_0}{B_0} = \frac{\sin^2 \alpha}{B}\,, \tag{3.44}$$

where B_0 is the magnetic field intensity at $\mathtt{P}_0$. On the contrary, the relationship between the azimuthal angles β and β_0 is not easily established. Nevertheless, a simple relation is obtained for particular values of β:

1. When $\beta = 0$ or π, $d_{\mathtt{P}}(\alpha, \beta) = 0$, i.e. the magnetic field line passing through P belongs to the drift shell of the observed proton. Consequently, $d_{\mathtt{P}_0}(\alpha_0, \beta_0) = 0$ and thus $\beta_0 = 0$ or π.

2. When $\beta = -\pi/2$, the drift shell of the observed proton is the most inner observable one. Since, in the magnetic equatorial plane, the drift shell shall remain the innermost one, $\beta_0 = -\pi/2$.

3. When $\beta = \pi/2$, the drift shell is the outermost observable one and $\beta_0 = \pi/2$.

For these particular cases, we the simple relation

$$\beta_0 = \beta \tag{3.45}$$

holds. The simplicity of Equation (3.45) is due to the choice of the coordinate system, the $\mathbf{n}$-axis of which is always perpendicular to the drift shells. With regard to the other approximations made previously, we assume that the validity of Equation (3.45) can be reasonably extended to the full range of the azimuthal angles.

From Equations (3.42)–(3.45), the variation of the shell parameter with the azimuthal angle β is approximatived by

$$\begin{aligned} \Delta L &= r_{\mathrm{g}0} \sin\beta \\ &= \frac{p}{q\sqrt{B_0 B_{\mathrm{m}}}} \sin\beta\,. \end{aligned} \tag{3.46}$$

The magnetic field intensities B_0 and B_{m} are related to the local values by the relations

$$\begin{cases} B_{\mathrm{m}} &= \dfrac{B}{\sin^2 \alpha} \\ \\ B_0 &= \dfrac{M}{L^3} \end{cases} \tag{3.47}$$

where $M = 0.311653\,\mathrm{Gauss}\,R_{\mathrm{E}}^{-3}$ is the magnetic moment used to compute the parameter L (McIlwain, 1961). In combination with Eq. (3.41), Eq. (3.46) provides a description of the unidirectional proton flux which includes the East-West asymmetry.

In this way, Eqs. (3.41) and (3.46) provide a new semi-empirical model for the description of the trapped proton anisotropy at low altitudes. In this model the dependence of the particle

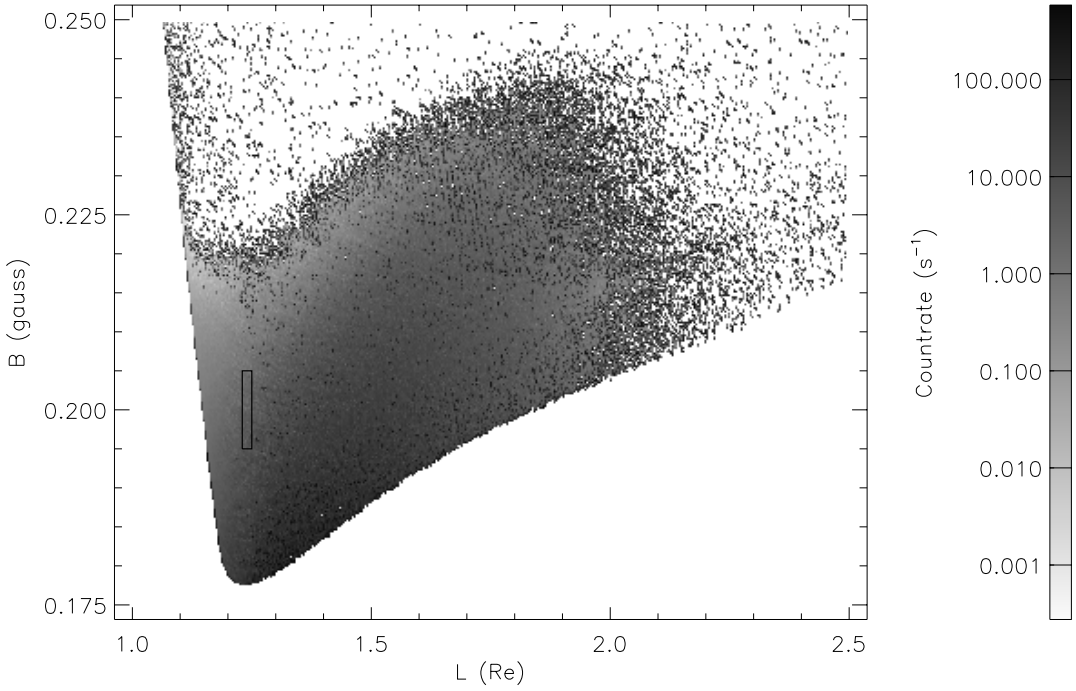

Figure 3.6. (B, L) diagram of the SAMPEX 86–120 MeV proton countrate. The rectangular box corresponds to the bin selected to test the new semi-empirical model.

flux on the azimuthal angle β is based on theoretical assumptions while the dependence on the pitch angle α has to be obtained empirically from a data set of measurements. This new semi-empirical model allows a complete description of the trapped proton fluxes at any location in the whole magnetosphere. Equation (3.41) can be re-written to highlight the main parameters:

$$f_{\mathrm{P}}(\alpha,\beta) = j_{\perp}(E, B_{\mathrm{m}}, L) + \left(\frac{\sqrt{E^2 + 2m_0c^2E}}{qc \quad \sqrt{MB_{\mathrm{m}}L^{-3}}}\right) \sin\beta \times \left.\frac{\partial j_{\perp}}{\partial L}\right|_{E,B_{\mathrm{m}}} \tag{3.48}$$

From Eq. (3.48), it clearly appears that the observed flux $f_{\mathrm{P}}(\alpha,\beta)$ is only a function of E, B_{m}, L, and β, where the perpendicular flux $j_{\perp}(E, B_{\mathrm{m}}, L)$ has to be determined from unidirectional measurements or models (e.g. the directional version of AP-8). On should note that the perpendicular flux model only depends on the particle energy E and drift shell labels (B_{m}, L).

3.3.4 Application to flux measurements

To complete the semi-empirical model, measurements of the directional proton flux in the radiation belts have to be available in order to determine $j_{\perp}$ and $\partial j_{\perp}/\partial L$. Three datasets of unidirectional proton fluxes in the SAA have been studied in TREND-3:

- AZUR/EI-88 with a field of view of $\pm 21°$;
- SAMPEX/PET with a field of view of $\pm 30°$;

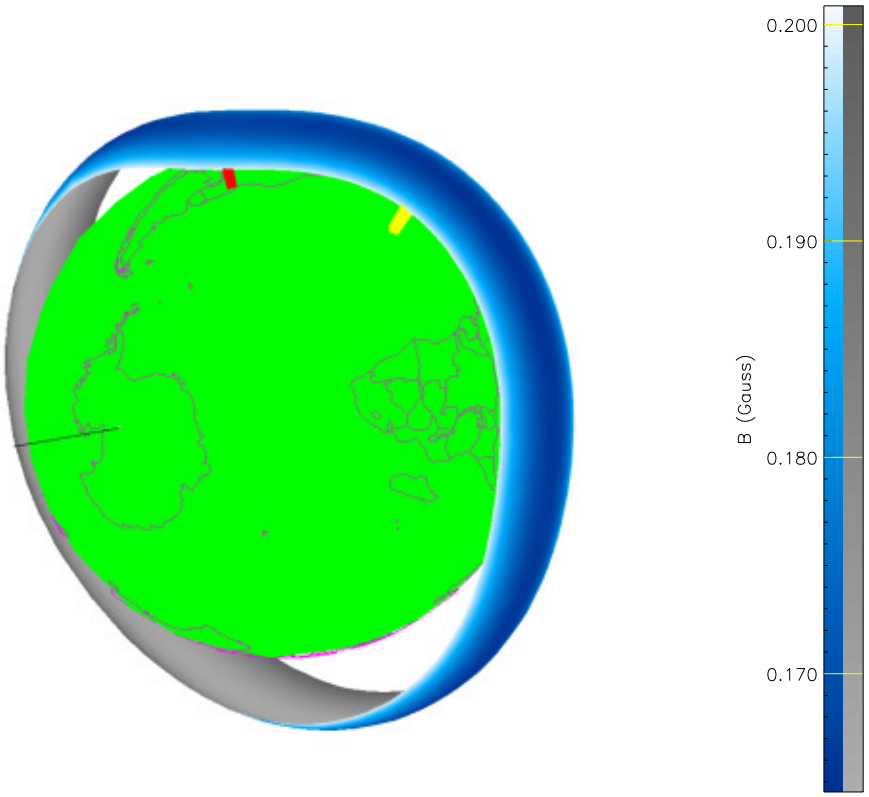

Figure 3.7. Representation of the magnetic drift shell $L = 1.24$, $B_{\rm m} = 0.2$. The two bars correspond to two mirror points in the southern hemisphere with a longitude of 51°W and 15°W, respectively. The IGRF 1995 magnetic field model has been used to trace the drift shell.

- UARS/HEPS with a field of view of $\pm 15°$.

A detailed description of these satellite missions and their instruments can be found in Chapters 4, 5, and 6, respectively. Unfortunately, up to now, only the PET data can be used to test and evaluate the new model, since

- a lack in the AZUR documentation prevents the computation of the azimuthal angle from the ephemeris data;
- the 3-axis stabilised attitude of the UARS spacecraft reduces the variation of β to a very small angle range for a fixed value of $B_{\rm m}$ and L.

As a test case for the new semi-empirical model, we have selected from the SAMPEX/PET data a bin in $(E, B_{\rm m}, L)$ space for the period of time which extends from mid 1994 to mid 1995. The bin is specified by

$$\begin{aligned} 0.195 < B_{\rm m} < 0.205\,, \\ 1.23 < L < 1.25\,, \\ 86.1 < E < 120.0\,. \end{aligned} \tag{3.49}$$

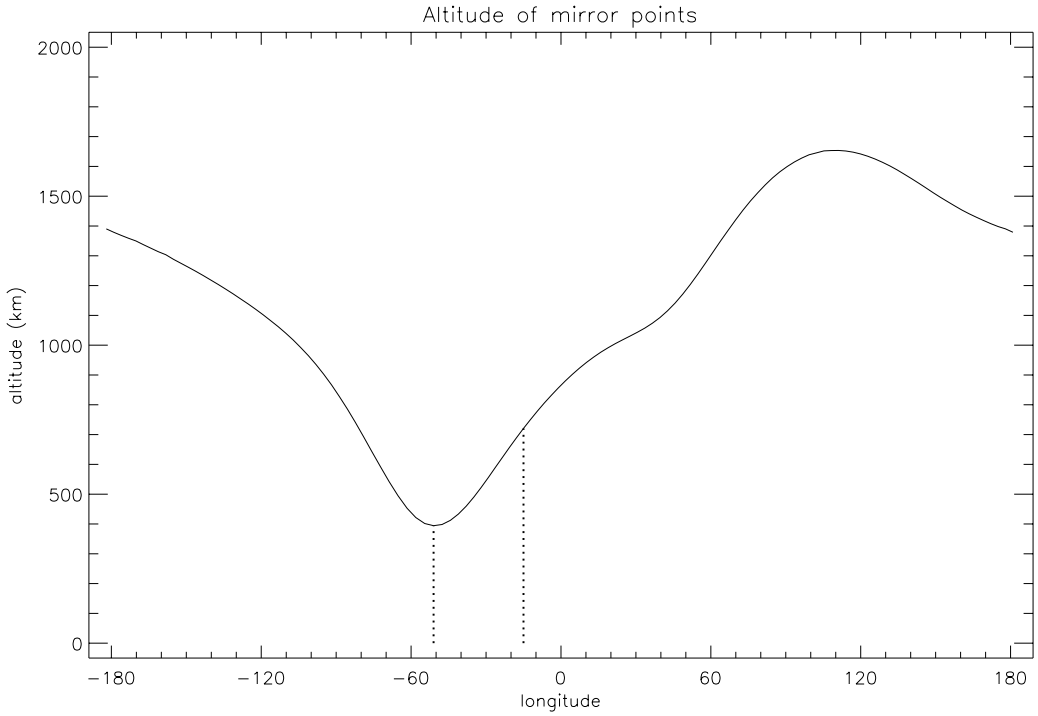

Figure 3.8. Geocentric altitude of the southern mirror points of the drift shell ($L = 1.24$, $B_{\rm m} = 0.2$) as a fonction of the mirror point longitude. The dotted lines indicate the mirror point with the lowest altitude (at 51°W of longitude) and an other mirror point located at 336.5 km higher (at 15°W of longitude).

The IGRF 1995 magnetic field model is used to evaluate the $B_{\rm m}$ and L values. The energy range corresponds to the channel `pen/p81` of the PET instrument (86–120 MeV). The Larmor radius at the mirror point corresponding to the central point of the bin specified by Eqs. (3.49) is equal to 77.2 km. The bin is represented on Fig. 3.6 where the countrates of the channel `pen/p81` are shown as a function of $B_{\rm m}$ and L.

The magnetic drift shell ($L = 1.24$, $B_{\rm m} = 0.2$) which corresponds to the central point of the selected SAMPEX data bin, is represented in a 3-D view in Fig. 3.7. The drift shell is clearly not axially symmetric and is mainly deformed near the SAA regio. The altitudes of the southern mirror points are shown on Fig. 3.8 as a function of the mirror point longitude. The lowest altitude on the shell is located at the mirror point 394.3 km, 25.7°S and 51.0°W. The location of this particular mirror point is indicated by the black bar in Fig. 3.7 and by a dotted line in Fig. 3.8. The variation of $L_{\rm GC}$ and the proton flux scale height are investigated below for this particular bin of data.

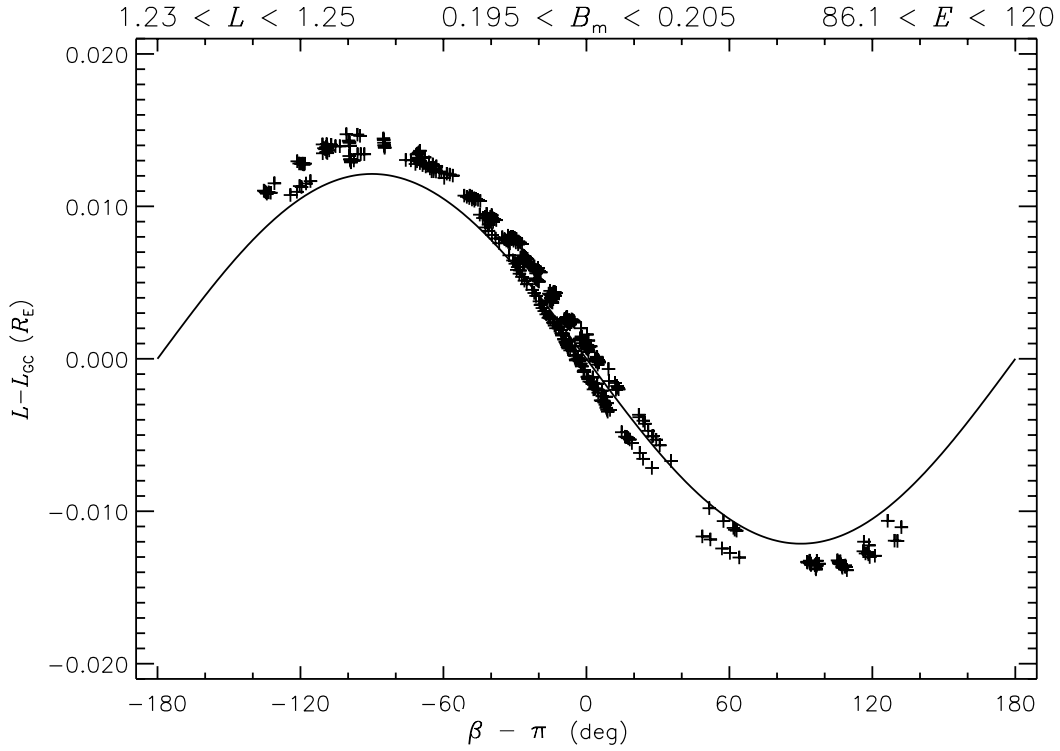

Figure 3.9. The variation ΔL of the shell parameter obtained in Eq. (3.46) as a function of the azimuthal angle β (solid curve) is compared to the difference $L - L_{\rm GC}$ obtained from the SAMPEX ephemeris (+ symbols) in the coordinate bin defined in the text.

3.3.4.1 Variation of $L_{\rm GC}$

Equation (3.46) predicts a variation of the shell parameter with respect to the azimuthal parameter given by

$$\Delta L = r_{\rm gm}\sqrt{\frac{B_{\rm m}}{B_0}}\sin\beta\,, \tag{3.50}$$

where $r_{\rm gm}$ and $B_{\rm m}$ are the gyroradius and magnetic field intensity at the mirror point. The validity of Eq. (3.46) or (3.50) depends only on the configuration of the magnetic field model. Instead of selecting, at random, geographic positions and look directions to evaluate the validity of these equations, we have used the SAMPEX ephemeris as a test case for the assumptions and approximations underlying Eq. (3.50).

For each point of the ephemeris in the bin defined by Eqs. (3.49), we have evaluated the shell parameter L as well as the value $L_{\rm GC}$ of the shell parameter at the guiding centre of 100 MeV protons. In Fig. 3.9, the difference $L-L_{\rm GC}$ is compared to the sinusoidal variation ΔL predicted by Eq. (3.46) for $B_{\rm m} = 0.20$ and $L = 1.24$. The relatively good agreement between ΔL and the ephemeris data validates the approximation in the determination of ΔL. The residual scattering of the ephemeris data is attributed to the scatter of $B_{\rm m}$ and L in the bin.

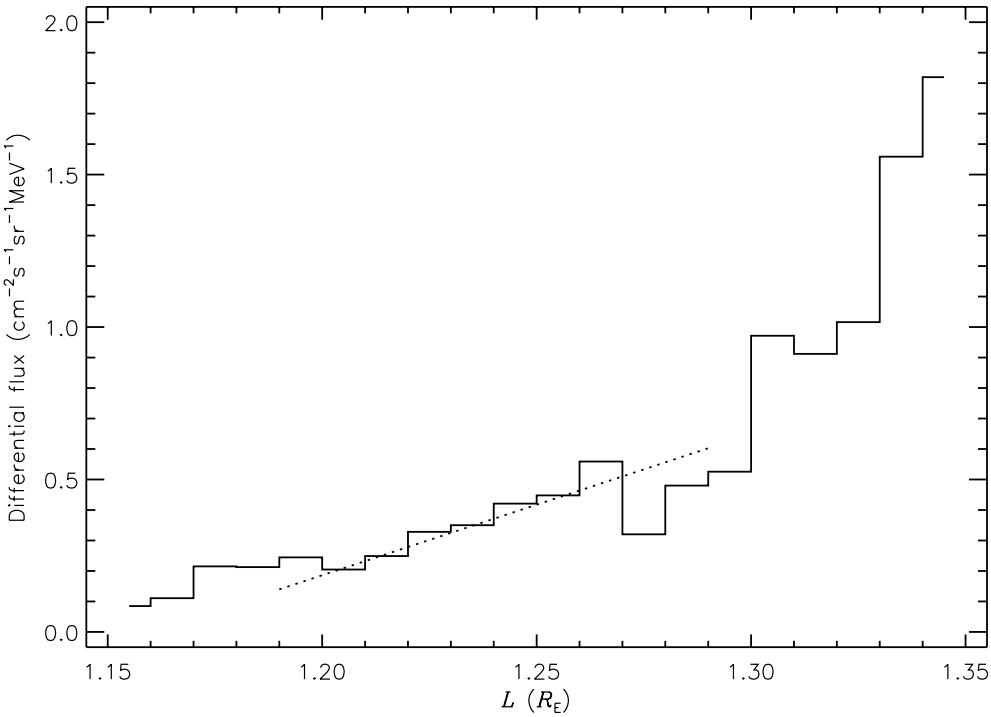

Figure 3.10. Dependence of the SAMPEX 86–120 MeV proton countrate on L for $0.195 < B_{\rm m} < 0.205$ and $|\sin\beta| < 0.05$. The dotted curve corresponds to a linear fit based on the data for which $1.23 < L < 1.25$.

3.3.4.2 Flux scale height

In order to apply the new semi-empirical model, the profile of the perpendicular flux with respect to L has to be determined. This profile will provide the two parameters of Eq. (3.41): $j_\perp$ and its derivative with respect to L.

The profile of the perpendicular flux as a function of the shell parameter L has been obtained by selecting the PET data for which $-0.05 < \sin\beta < 0.05$, $0.195 < B_{\rm m} < 0.205$ and $1.15 < L < 1.35$. The selection on $\sin\beta$ retains those measurements with $L_{\rm GC}$ values close to L, so that $j_\perp$ is well approximated by the mean of the selected fluxes, and that a linear fit can be used to determine $\partial j_\perp/\partial L$. Figure 3.10 shows the dependence on L of the proton countrate of the data points that meet the above conditions. Due to the small livetime of the PET measurements, and the corresponding poor statistics, the data in Fig. 3.10 have been binned in twenty L bins between $L = 1.15$ and 1.35. The problem relative to small livetimes is specific to the PET data and is discussed in detail in Technical Note 5, Part II.

Figure 3.11 shows a "zoom" of Fig. 3.10 around $L = 1.24$. The data points have again been binned in twenty L bins, now between $L = 1.23$ and 1.25. A linear fit of the binned flux of Fig. 3.11 is used to evaluate the flux at $L = 1.24$ and the value of its derivative. The linear fit is

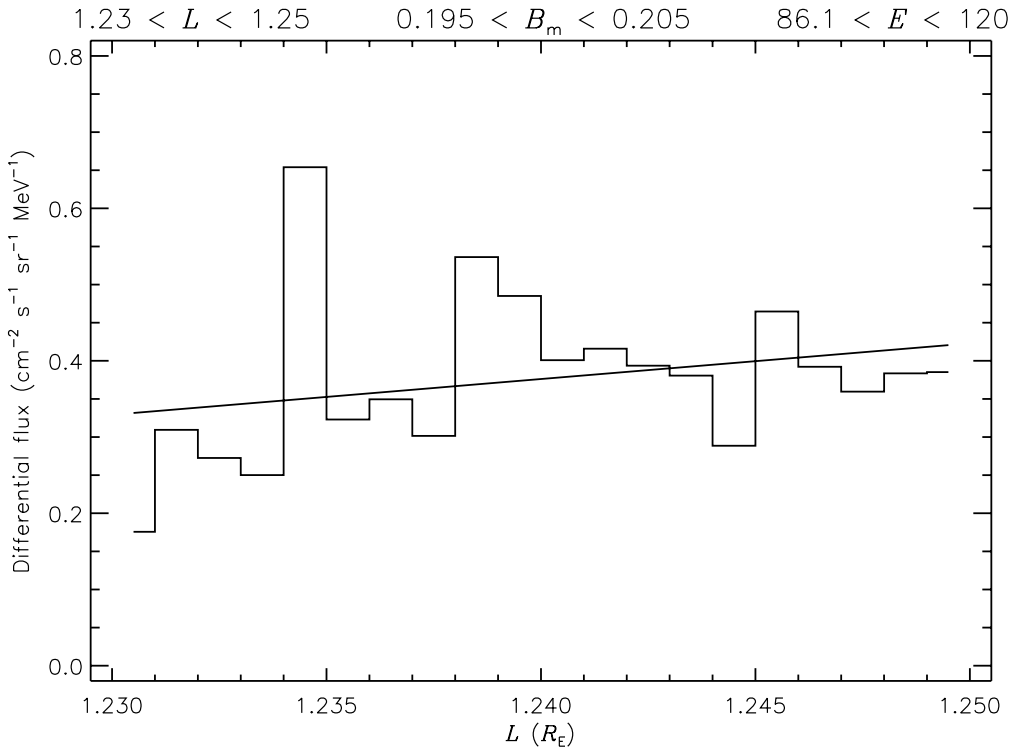

Figure 3.11. Dependence of the SAMPEX 86–120 MeV proton countrate on L for $0.195 < B_{\rm m} < 0.205$, $1.23 < L < 1.25$ and $|\sin\beta| < 0.05$. The solid line corresponds to a linear fit.

given by

$$j_\perp = 0.375\,\mathrm{cm}^{-2}\mathrm{s}^{-1}\mathrm{sr}^{-1}\mathrm{MeV}^{-1}, \qquad \frac{\partial j_\perp}{\partial L} = 4.63\,\mathrm{cm}^{-2}\mathrm{s}^{-1}\mathrm{sr}^{-1}\mathrm{MeV}^{-1}R_{\rm E}^{-1}\,. \tag{3.51}$$

The linear fit is represented on Figs. 3.10 and 3.11 by a dotted line and a solid line, respectively. One should note the large scattering of the binned data around the linear fit. The scattering is related to the Poisson statistic behaviour of the PET measurements. Unfortunately this behaviour complicates the evaluation of the new semi-empirical model.

3.3.4.3 East-West asymmetry

For the bin defined by Eqs. (3.49), we have evaluated the dependence of the observed flux on the azimuthal angle β. In Fig. 3.12, the flux obtained with Eq. (3.41) is compared to the SAMPEX/PET measurements in the selected bin. As before, the data points have been binned, now in twenty β bins. Note that the bins around $\beta = 0^\circ$ are empty.

Now that the dependence on L of the perpendicular flux is determined, Eq. (3.41) can be used to evaluate the East-West asymmetry effect. The East-West effect predicted by the new semi-empirical model is a sine curve, which is represented in Fig. 3.12 as a solid line. The main trend of the binned data is well rendered by the sine curve. Nevertheless the scatter

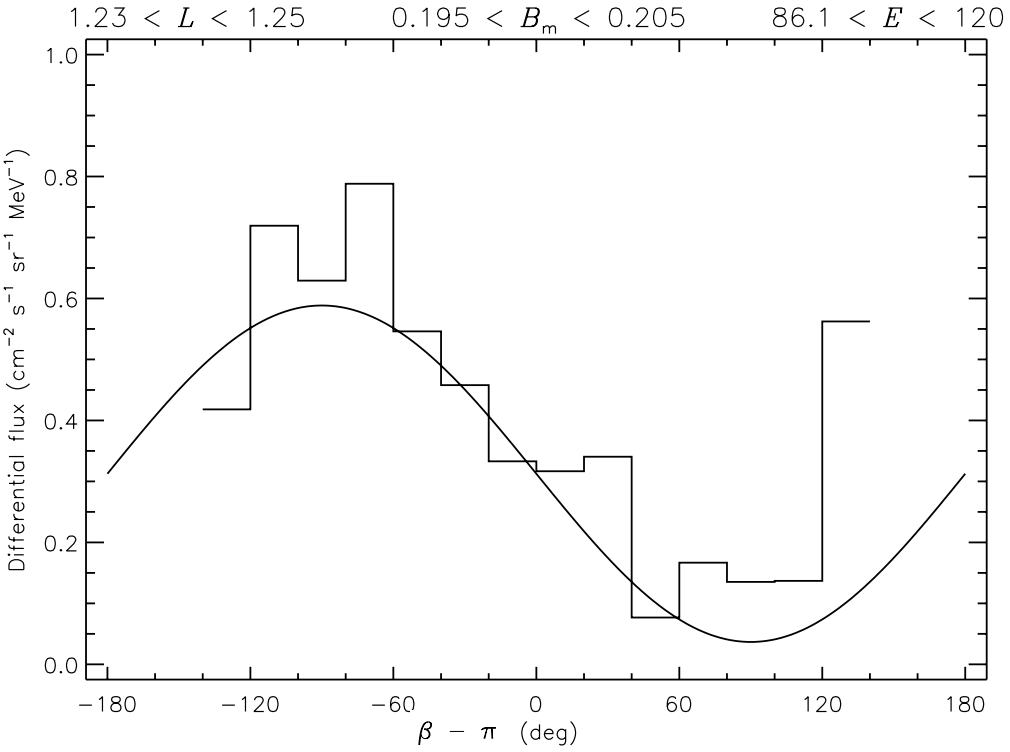

Figure 3.12. Dependence of the SAMPEX 86–120 MeV proton countrate on the azimuthal angle β for the points in the bin ($0.195 < B_{\rm m} < 0.205$, $1.23 < L < 1.25$), i.e. the same points as Fig. 3.9. The solid curve corresponds to the linear fit of Fig. 3.11 where ΔL is obtained from Eq. (3.46).

around the sine curve is large. Part of the scattering is due to the finite size of the bin in B, L, and energy. Further uncertainties are introduced by the relatively large opening angle ($60°$)of the PET instrument which creates an uncertainty on the angles α and β. Finally, the saturation problem of the PET (see Technical Note 5), resulting in low proton count rates, adds an inherent uncertainty factor. The combined data scatter prohibits a quantitative assessment of the model. Therefore, comparisons of the model to the directional dependence of PET data in other bins will probably not improve the validation. Morever, even with one year of data, the coverage in β is not complete in all (B, L) bins.

3.4 Intercomparison of the anisotropy models

3.4.1 Angular distribution predicted by VF1-MIN and BK-MIN models

Two examples of angular distributions obtained with the VF1MIN and BK-MIN models are presented in Figs. 3.13–3.16, which correspond to the differential trapped proton flux predicted at two different points of observation $\bar{p}$ and $\bar{q}$ in the South Atlantic Anomaly. Both points are located at 60°W and 35°S, with altitudes of 450 km and 1,500 km, respectively.

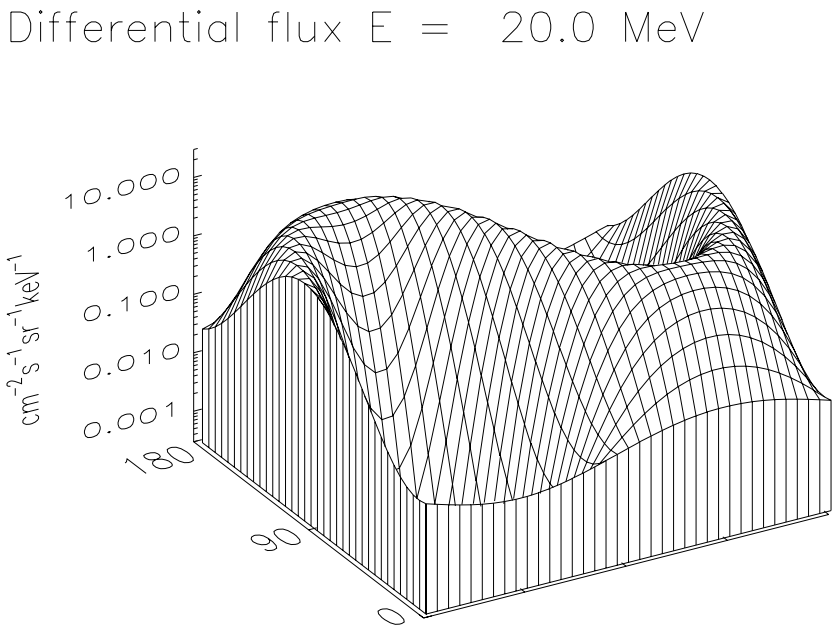

Figure 3.13. VF1MIN predicted anisotropy of trapped proton differential flux at 60° W, 35° S and altitude 450 km. The proton energy is set to 20 MeV and the omnidirectional flux is fixed to 12.5 $\mathrm{cm}^{-2}\mathrm{s}^{-1}\mathrm{keV}^{-1}$. The coordinate system is fixed relatively to the zenith direction (z-axis) and the local magnetic East direction.

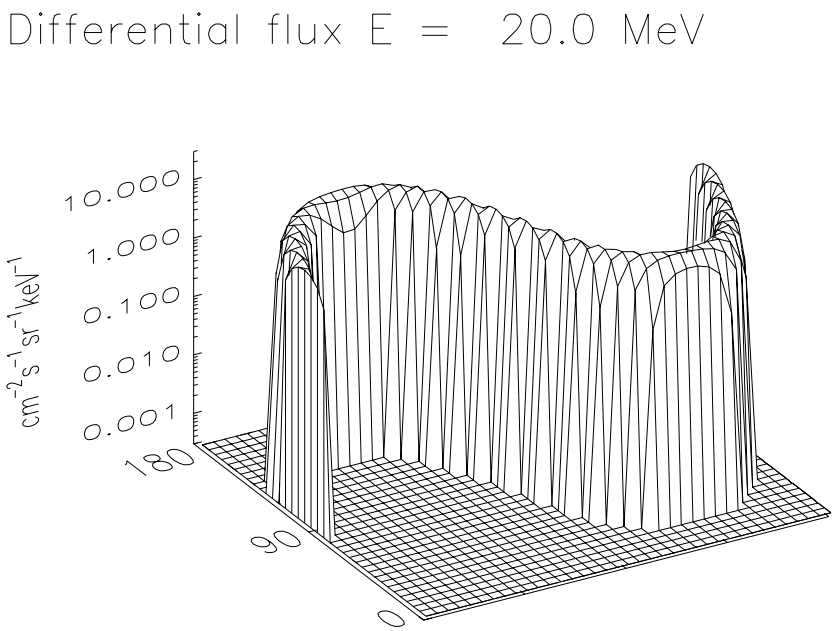

Figure 3.14. BK-MIN predicted anisotropy of trapped proton differential flux at 60° W, 35° S and altitude 450 km. The proton energy is set to 20 MeV and the omnidirectional flux is 12.5 $\mathrm{cm}^{-2}\mathrm{s}^{-1}\mathrm{keV}^{-1}$. The coordinate system is fixed relatively to the zenith direction (z-axis) and the East direction.

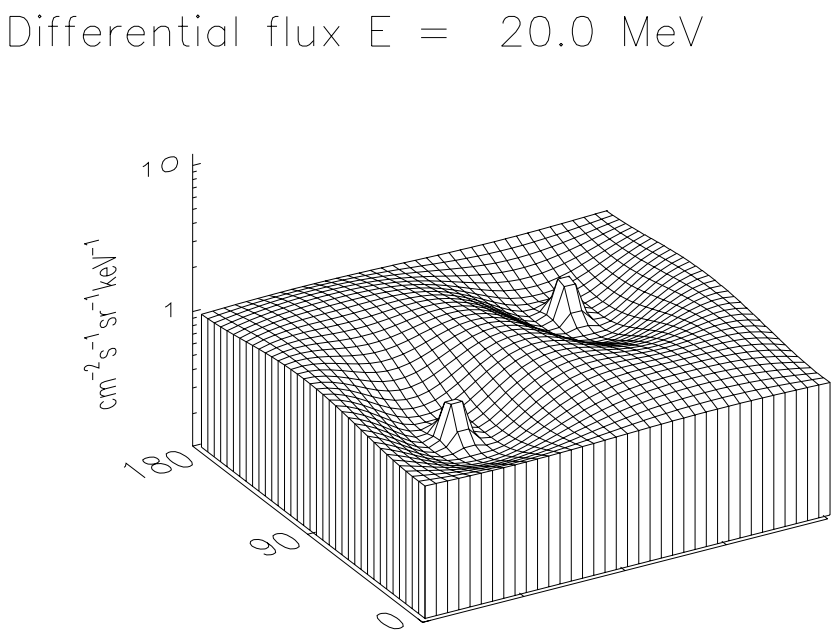

Figure 3.15. Same as Fig. 3.13 but for an altitude of 1500 km based on the VF1MIN model.

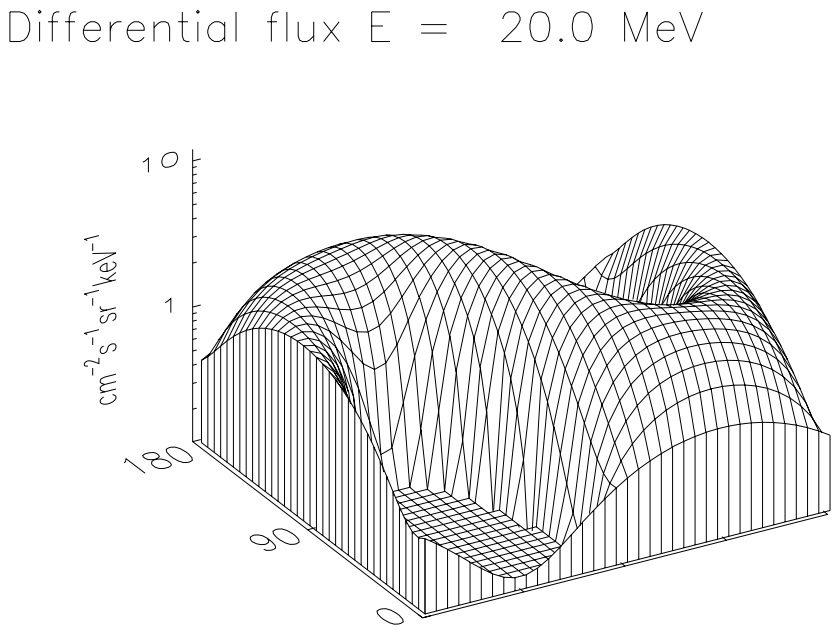

Figure 3.16. Same as Fig. 3.14 but for an altitude of 1500 km based on the BK-MIN model.

Table 3.2. Magnetic coordinates (B, L), magnetic dip angle I, parameter σ and scale height $H^{\min}$ for two points of observation. The (B, L) coordinates are obtained using the Jensen and Cain (1962) geomagnetic field model.

location	B (gauss)	L	I (deg)	σ (deg)	$H^{\min}$ (km)	$\alpha_{\rm L}$ (deg)
60°W, 35°S, 450 km	0.2210	1.28	33.6	10.3	108.1	79.5
60°W, 35°S, 1500 km	0.1551	1.47	35.2	37.4	1677.2	51.0

We use an orthogonal coordinate system defined as follows:

- the z-axis points to the zenith (corresponds to $\bar{1}_R$ in Fig. 3.1);
- the y-axis is defined by the intersection of the mirror plane and the horizontal plane; it points in the eastward direction (corresponds to $\bar{1}_y$ in Fig. 3.1);
- the x-axis is defined by the intersection between the mirror plane and the local vertical plane which contains the magnetic field line (corresponds to $\bar{1}_H$ in Fig. 3.1).

We consider protons with energy E =20 MeV and an omnidirectional differential flux of 12.5 cm^{-2}s^{-1}keV^{-1}. The Jensen and Cain (1962) geomagnetic field model was used to obtained the (B, L) coordinates. The magnetic coordinates (B, L), the magnetic dip angle I, the parameter σ, the scale height $H^{\min}$ and the Badhwar & Konradi (1990) loss cone angle $\alpha_{\rm L}$ are given in Table 3.2.

3.4.1.1 Angular distribution at 450 km altitude

The predicted angular distributions observed at the point $\bar{p}$ corresponding to an altitude of 450 km are presented in Figs. 3.13 and 3.14, respectively, for the VF1MIN and BK-MIN models. The unidirectional differential fluxes are presented as a function of the polar and azimuthal angles. It can be seen that the angular variations of the unidirectional differential flux are quite different in Figs. 3.13 and 3.14. In Fig. 3.13, the angular distribution has two deep valleys centred respectively around the polar angles 56° and 124° and azimuthal angles 90° and 270°. These two directions correspond to the directions of the magnetic field line. The angular distribution found with the BK-MIN model, shown in Fig. 3.14, is much steeper than that corresponding to the VF1MIN model and looks like a sheer ridge. In other words, a narrower angular distribution is obtained with the BK-MIN model than with the VF1MIN model.

The pitch-angle distribution of the BK-MIN model is more sharply peaked than the one corresponding to the VF1MIN model. In the BK-MIN model, based on Badhwar and Konradi's (1990) approximation, the loss cone is defined explicitly in terms of the angle $\alpha_{\rm L}$. At the point $\bar{p}$, $\alpha_{\rm L}$ =79.5° and the unidirectional flux is confined to a cone of 21° opening angle. On the other hand, in the Heckman and Nakano (1969) description used in the VF1MIN model, the loss

cone is defined implicitly through the parameter[4] σ. At the point $\bar{p}$, σ =10.3° which induces a smoother anisotropy than the Badhwar and Konradi (1990) pitch-angle distribution. At α =90°, the differential flux predicted by the VF1MIN model is lower than that predicted by the BK-MIN model due to the normalisation with respect to the omnidirectional flux [see Sect. 3.2.4, Eq. (3.20)].

Since the parameter $\alpha_{\rm L}$ is obtained from a fit of the AP-8 MIN unidirectional flux database (see Sect. 3.2.2.3), the results obtained with the BK-MIN model are a better approximation for the AP-8 MIN trapped proton model than those obtained with the VF1MIN model.

3.4.1.2 Angular distribution at 1,500 km altitude

The angular distributions of the unidirectional differential flux predicted at the second point, $\bar{q}$ (with altitude 1,500 km), are presented in Figs. 3.15 and 3.16, respectively, for the VF1MIN and BK-MIN models. The shape of the angular distribution for both models is quite different from that for altitude 450 km illustrated in Figs. 3.13 and 3.14.

The valleys in Fig. 3.15 are shallower than in Fig. 3.13 as a result of an increase of the parameter σ from 10.3° to 37.4°. However, unexpected peaks appear in the centre of both valleys at pitch-angles of 0° and 180°. They are caused by the singularity in the conversion factor $W_{\rm VF}$ of Eq. (3.32). Indeed, when $\sin\alpha$ tends to zero, Expression (3.32) diverges. The singularity is a consequence of the particular normalisation method chosen by Watts et al. (1989) [see Eq. (3.32)]. This divergence should have appeared already at the lower altitude ($\bar{p}$), i.e. in Fig. 3.13 where σ =10.3°. But in this case the value of the gaussian $\exp[-(90^\circ-\alpha)^2/2\sigma^2]$ in Eq. (3.32) becomes very small when α is near 0° or 180°, and consequently the divergence of $W_{\rm VF}$ is masked. In contrast, at $\bar{q}$ where σ =37.4°, the value of the gaussian is much larger and the divergence of Eq. (3.32) is emphasized; therefore the two peaks clearly appear in the directions parallel and anti-parallel to the magnetic field direction.

At low altitude, where the parameter σ is small, this singularity does not appear. Therefore, when the altitude of observation exceeds 1,000 km, the VF1MIN and VF1MAX models should not be used.

In the BK-MIN model, the extension to a higher altitude does not cause any problems. The loss cone angle at the point $\bar{q}$ is about 51° and the ridge seen in Fig. 3.14 flattens out in Fig. 3.16. In other words, the pitch-angle distribution and the East-West asymmetry become less anisotropic. However, the fact that two deep holes remain proves that at 1,500 km altitude the anisotropy of the trapped proton flux is still important.

3.4.2 Comparison with the semi-empirical model

In this section, we compare the new semi-empirical model described in Sect. 3.3 to the model of Watts et al. (1989) and to the BK-MIN model. For the sake of clarity, the omnidirectional

[4]The pitch-angle distribution is described with the help of a gaussian of which σ is the half-width parameter (see Sect. 3.2.2.1).

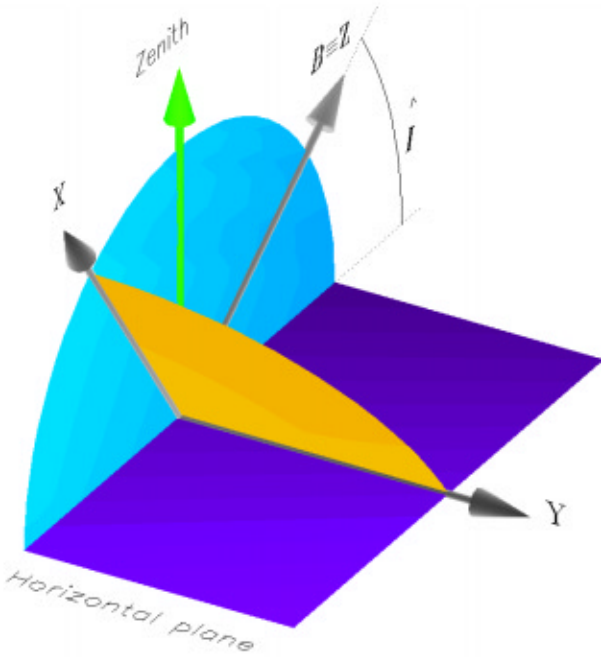

Figure 3.17. Representation of the coordinate system used to compare different proton anisotropy models

fluxes of the latter two models are normalized to unity, and the look directions are determined in a coordinate system such that

1. the Z-axis is parallel to the magnetic field vector;
2. the Y-axis lies in the local horizontal plane and points in the magnetic East direction;
3. the plane XZ contains the zenith direction, i.e. it is a local vertical plane;
4. the plane XY corresponds to the local mirror plane.

The coordinate system is represented in a 3-D view on Fig. 3.17. The representation in Fig. 3.17 includes the local horizontal plane, the local mirror plane and the local vertical plane which contains the magnetic field vector. Note that the coordinate system (Z, X, Y) differs from the coordinate system ($\mathbf{e}$, $\mathbf{n}$, $\mathbf{b}$) [defined in Sect. 3.3.2] by a rotation about the Z-axis only, i.e. the azimuthal angle ϕ differs from the angle β by an offset. The value of this offset depends on the magnetic field configuration, and thus on the geographic position.

The conversion factors $W_{\mathrm{HN-LS}}$, $W_{\mathrm{BK-LS}}$ and $W_{\mathrm{BK-beta}}$ of the three models, are compared at two geographic locations: (394.3 km, 25.7°S, 51.0°W) and (720.8 km, 7.9°S, 15.0°W), i.e. the two mirror points on the drift shell $L = 1.24$, $B_{\mathrm{m}} = 0.2$, shown in Fig. 3.7. Both points are highlighted on Figs. 3.7 and 3.8 and have been used already to compare the two pitch-angle distributions f_{HN} and f_{HN}.

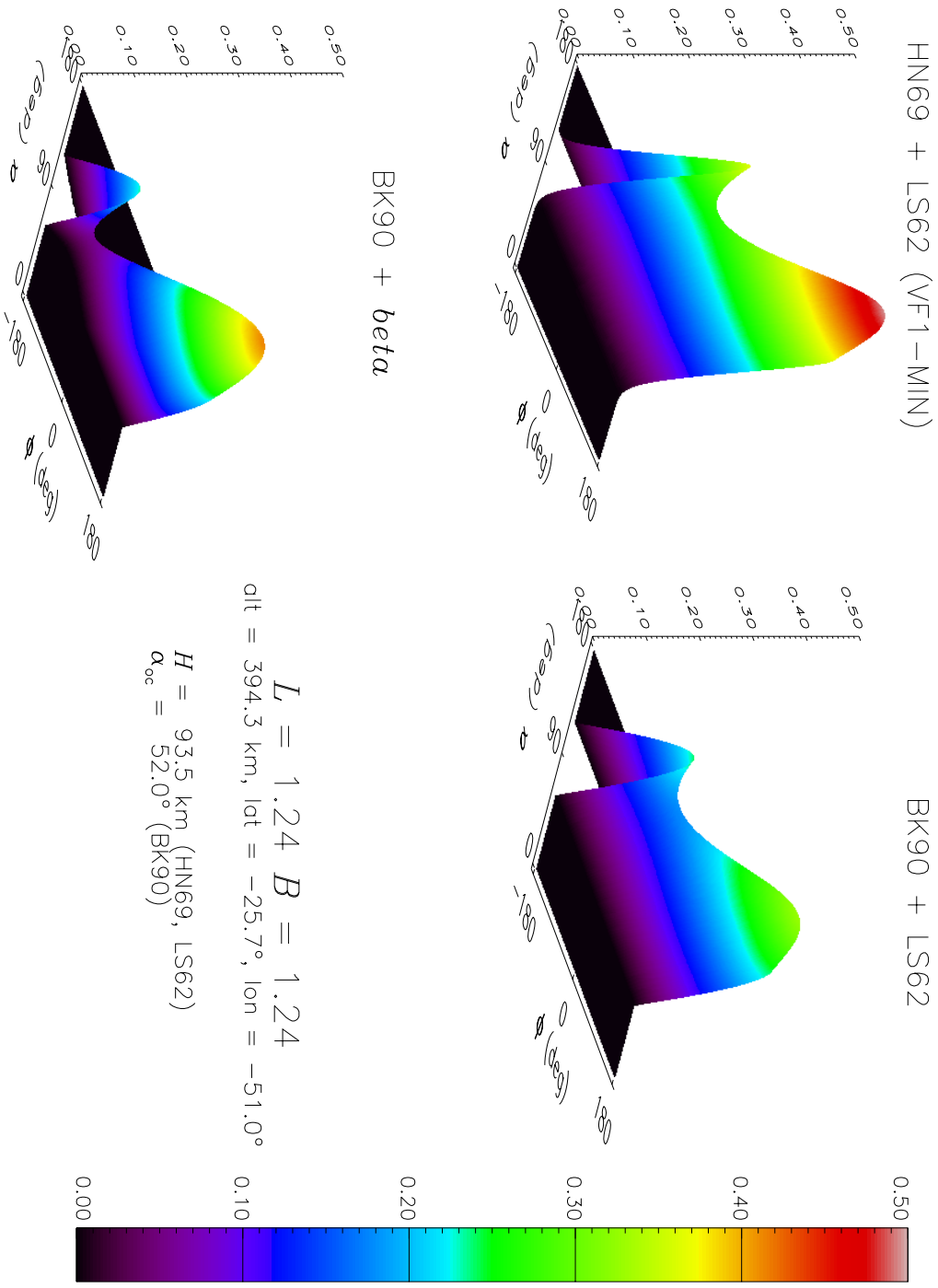

Figure 3.18. Dependence of the directional 100-MeV proton flux on the polar and azimuthal direction at the position (394.3 km, 25.7° S, 51.0° W)

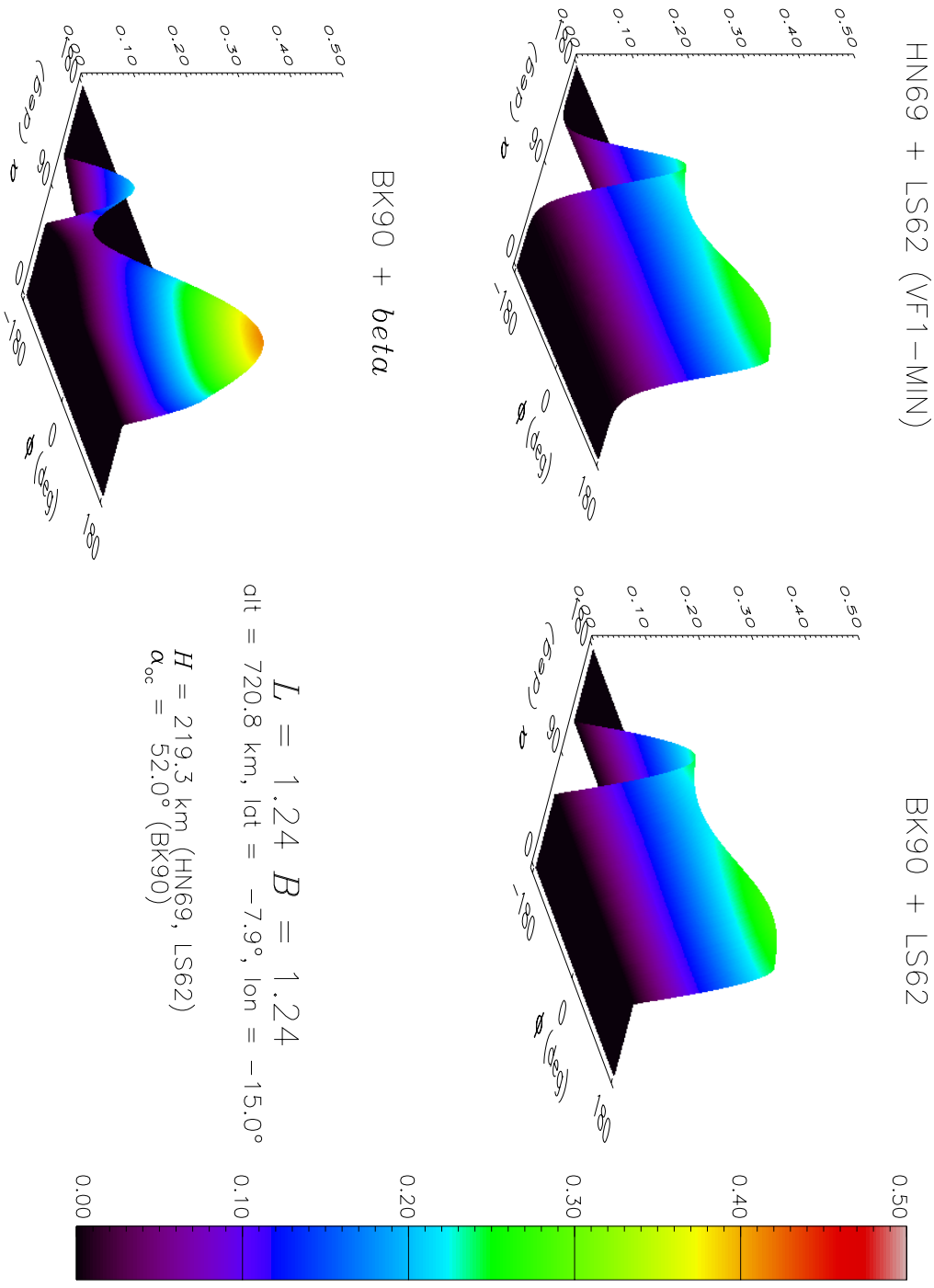

Figure 3.19. Dependence of the directional 100-MeV proton flux on the polar and azimuthal direction at the position (720.8 km, 7.9°S, 15.0°W)

In Figs. 3.18 and 3.19, the dependences of the flux on the polar and azimuthal angles (α, ϕ) predicted by both models are compared at the two geographic locations for 100 MeV protons. Only the conversion factors $W_{\mathrm{HN-LS}}$, $W_{\mathrm{BK-LS}}$, and $W_{\mathrm{BK-beta}}$ are represented on both figures. In Fig. 3.18, which corresponds to the lowest mirror point, the East-West asymmetry is apparent for the three models. One should note that the new semi-empirical model is more asymmetric than the two others.

In Fig. 3.19, the asymmetry is much reduced for the $W_{\mathrm{HN-LS}}$ and $W_{\mathrm{BK-LS}}$ functions. This reduction is due to the variation by a factor $7/3$ of the atmospheric scale height between 394 and 721 km of altitude. On the other hand, the asymmetry of the new semi-empirical model remains unchanged. Between Fig. 3.18 and Fig. 3.19, the function $W_{\mathrm{BK-beta}}$ has not changed except by a small shift in the azimuthal angle due to a variation of the offset between the angles β and ϕ.

3.5 ANISO software overview

The software package `UNIRAD` (Heynderickx et al. 1996d) is a suite of programs developed for ESA for evaluating the radiation fluences and doses experienced by a spacecraft along its orbit.

This section is devoted to the implementation of the trapped proton anisotropy models VF1-MIN, VF1-MAX, BK-MIN and BK-MAX in the `UNIRAD` package. This implementation consists mainly in a program called `ANISO` which allows to calculate the trapped proton unidirectional fluences observed for a given orbit and a given direction $\bar{D}$ of the detector view angle, both are input parameters specified by the user.

The unidirectional fluences are obtained by the transformation of the omnidirectional differential flux into an unidirectional flux along the orbit. The unidirectional differential flux is then averaged over the whole orbit to provide an unidirectional fluence.

One should note that the ANISO software does not implemented the generalized anisotropy model presented in Section 3.3.

The implementation of `ANISO` does not modify the use of `UNIRAD` when the East-West anisotropy is bypassed. Part of the flow diagram of the new `UNIRAD` package is represented in Fig. 3.20. This diagram illustrates the interdependence between different program elements. The original set of `UNIRAD` programs has been grouped on the left hand part of the diagram. Except for `PROJECT.SHP`, the other output files are not shown. The right hand part of the diagram corresponds to the inputs and output of the `ANISO` program. The `PROJECT.INT` and `PROJECT.MAT` files contain the ephemeris and attitude of the satellite or view angles of the particle detectors. The magnetic field vector and the omnidirectional integral fluxes are provided to `ANISO` through the `PROJECT.SPP` file generated by `TREP`. The output file `PROJECT.TRD` contains the orbit averaged unidirectional integral and differential fluences. The structure of the file `PROJECT.TRD` is similar to that of the file `PROJECT.TRI` and is described in Table 3.5.

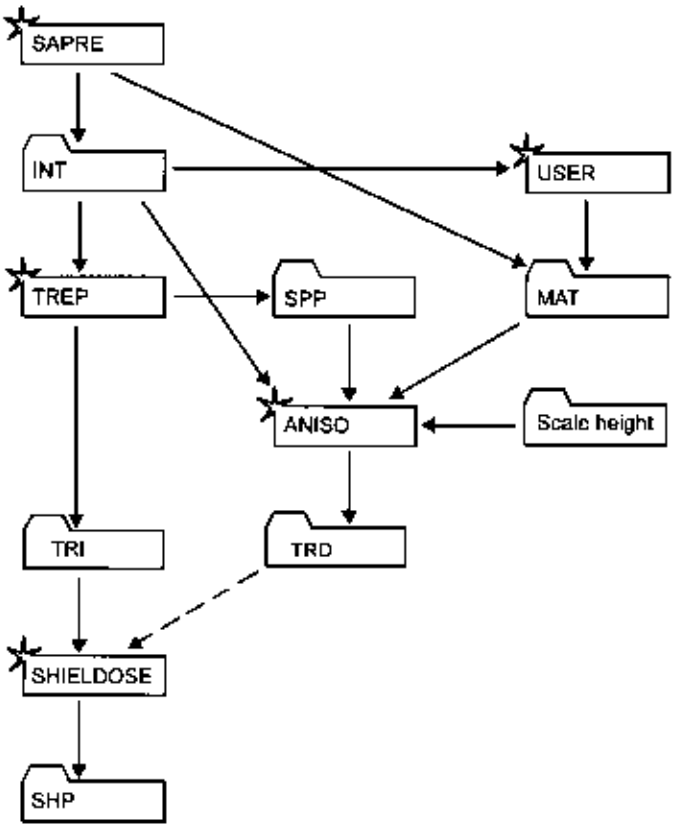

Figure 3.20. Flow diagram of UNIRAD

3.5.1 Attitude interface file

The attitude interface file PROJECT.MAT is an input of ANISO which contains the attitude of the satellite along its orbit. This file may be generated by SAPRE for the three cases listed in Sect. 3.5.1.1. For other cases, the file PROJECT.MAT must be produced by the user as an input.

The attitude interface file PROJECT.MAT is in Fortran unformatted format, with fixed record length of 80 bytes, in direct access. Each record corresponds to an orbital point in the common interface file (PROJECT.INT). The structure of the attitude interface file is given in Table 3.3. The rotation matrix is given by

$$[A(i,j)] = \begin{bmatrix} \bar{1}_R \cdot \bar{1}_x & \bar{1}_R \cdot \bar{1}_y & \bar{1}_R \cdot \bar{1}_z \\ \bar{1}_\theta \cdot \bar{1}_x & \bar{1}_\theta \cdot \bar{1}_y & \bar{1}_\theta \cdot \bar{1}_z \\ \bar{1}_\phi \cdot \bar{1}_x & \bar{1}_\phi \cdot \bar{1}_y & \bar{1}_\phi \cdot \bar{1}_z \end{bmatrix} \tag{3.52}$$

where $(\bar{1}_x, \bar{1}_y, \bar{1}_z)$ is the coordinate system attached to the satellite and $(\bar{1}_R, \bar{1}_\theta, \bar{1}_\phi)$ is the geocentric spherical coordinate system. The unit vector $\bar{1}_R$ points to the zenith. The unit vectors $\bar{1}_\theta$ and $\bar{1}_\phi$ lie in the horizontal plane, pointing respectively to the geographic South and East directions.

Table 3.3. Record structure of the interface file PROJECT.MAT determining the attitude of particle detector or the view angle directions

Word	Data Type	Description
1–9	REAL*8	Rotation matrix describing the satellite attitude relative to the geographic spherical axis $(\bar{1}_R, \bar{1}_\theta, \bar{1}_\phi)$ at the current location of the satellite
10	REAL*8	Angle between the zenith direction and the satellite velocity vector (degrees)

3.5.1.1 Changes implemented in the SAPRE program

The SAPRE program has been modified to generate simple attitude interface files. This new feature is controlled by the new namelist parameter IATTI (INTEGER*4). The default value is set to 0; in this case no attitude interface file is generated. When IATTI is set to a positive value, a PROJECT.MAT file is generated by SAPRE. The file contains the attitude of the satellite which corresponds to one of the 3 orientations of the satellite:

IATTI =**1** The z-axis of the satellite points to the zenith. The x-axis and y-axis are in the horizontal plane pointing respectively to the geographic North and West directions.

IATTI =**2** The z-axis is parallel to the velocity vector of the satellite. The x-axis lies in the orbital plane pointing away from the Earth. The y-axis is perpendicular to the orbital plane, pointing to the South.

IATTI =**3** The $(\bar{1}_x, \bar{1}_y, \bar{1}_z)$ coordinate system is parallel to the geographic equatorial inertial coordinate system.

When different SAPRE namelists are present in the same file PROJECT.NML, IATTI has to be either equal to zero in every namelist, or always greater than zero. In other words, trajectories with and without ANISO calculations should not be mixed.

3.5.2 ANISO program

The ANISO program transforms trapped proton omnidirectional integral fluxes produced by TREP into orbit-averaged unidirectional integral and differential fluences. The program may also provide the unidirectional integral or differential fluxes along the orbit of the satellite. The transformation is based on the trapped proton anisotropy models described in Sect. 3.2.5 and 3.2.6. The ANISO program takes as input the namelist ANISO and reads the geodetic and (B, L) coordinates from the common interface file PROJECT.INT, the satellite attitude from the attitude interface file PROJECT.MAT, the magnetic field vector components and the full proton flux spectrum from the file PROJECT.SPP.

Table 3.4. ANISO Namelist parameters

Parameter	Type	Default	Function
JANIS	I*4	1	Anisotropy model identification number 1: VF1MIN model (Watts et al., 1990) 2: VF1MAX model (Watts et al., 1990) 3: BK-MIN model (Badhwar and Konradi, 1990) 4: BK-MAX model (Badhwar and Konradi, 1990)
NDIR	I*4	180	Number of look directions (12×15)
DALPH	R*4(400)		Polar angle for each look direction in degrees. Default: DALPH$(j + 15 * i + 1) = 7.5 + 15i$ where i varies from 0 to 11 and j from 0 to 14.
DBETA	R*4(400)		Azimuthal angle for each look direction in degrees. Default: DBETA$(j + 15 * i + 1) = 24j$ where i varies from 0 to 11 and j from 0 to 14.
XOMEGA	R*4(400)	0	Solid angle (sr) for each look direction. When XOMEGA is set to zero, XALPH and XBETA are used as polar and azimuthal opening angle to compute the solid angle.
XALPH	R*4(400)	15	Polar opening angle, in degrees
XBETA	R*4(400)	24	Azimuthal opening angle, in degrees
IFULL	I*4	0	When IFULL is greater than zero, the spectrum file PROJECT.SPD is generated.

The namelist parameters controlling the program ANISO are listed in Table 3.4. The polar and azimuthal angles DALPH and DBETA are defined in the coordinate system $(\bar{1}_x, \bar{1}_y, \bar{1}_z)$ attached to the satellite.

Please note that the trapped proton anisotropy models have to be used with the appropriate omnidirectional spectra. VF1MIN and BK-MIN make use of the model AP-8 for solar minimum[5] while VF1MAX and BK-MAX are defined for solar maximum[6]. ANISO produces a warning when the omnidirectional model and the anisotropy model are not consistent with each other.

The file PROJECT.TRD produced by ANISO contains the orbit-averaged integral and differential spectra of trapped protons for the different look directions defined by (DALPH =

[5]In the TREP namelist, the omnidirectional AP-8 MIN model is correctly selected by the settings: SOLACT = 'MIN', OMNI = 1 and ISPEC = 1. The (B, L) coordinates are then computed with the Jensen and Cain (1962) geomagnetic model.

[6]In the TREP namelist, the omnidirectional AP-8 MAX model is correctly selected by the settings: SOLACT = 'MAX', OMNI = 1 and ISPEC = 1. The (B, L) coordinates are then computed with the GSFC 12/66 (Cain et al., 1967) geomagnetic model updated to epoch 1970.

Table 3.5. Format of the file `PROJECT.TRD`. When more than one trajectory is specified, the whole structure is repeated.

Record	Format	Description
1	`1X,A80`	Project header
2	`5H E-W ,A8`	Omnidirectional trapped proton model header
3	`1X,A32`	Header of the internal geomagnetic field model
4	`1X,A32`	Header of the external geomagnetic field model
5	`I3,3X,I3,3X, F8.1,12X,I3`	Numbers of internal and external field models, epoch for internal magnetic field model and number of look directions
6	`F6.1,2F8.1`	Orbit inclination (deg), perigee height (km) and apogee height (km)
7	`34X,E11.4, 4X, A6`	Total orbit time (hrs) and anisotropy model header
8	`2F10.5`	Polar and azimuthal angle (degrees) of the first look direction
9	`2F10.5, F20.6`	Polar and azimuthal opening angle (degrees) and solid opening angle ($100 = 4\pi$ sr)
10	`I4,16X,2I4`	Number of energies (`NENERP`) in trapped proton spectra, index of the look direction and number of look directions
11	`3E11.4`	Proton energy (MeV), integral ($\mathrm{cm}^{-2}\mathrm{s}^{-1}$) and differential ($\mathrm{cm}^{-2}\mathrm{s}^{-1}\mathrm{keV}^{-1}$) flux
⋮		⋮
10+`NENERP`	`3E11.4`	Proton energy, integral and differential flux
11+`NENERP`		Blank line
12+`NENERP`		Blank line
13+`NENERP`		Blank line
14+`NENERP`		Same as lines 8–(13 + `NENERP`) for the second look direction
⋮		⋮

ζ, `DBETA` $= \eta$). The format of the file is described in Table 3.5. For each look direction, the orbit-averaged trapped proton differential spectra is evaluated as

$$\bar{j}(E,\zeta,\eta) = \frac{\Delta\Omega}{\sum_{\bar{p}} \delta t(\bar{p})} \sum_{\bar{p}} W(E,\bar{p},\zeta,\eta) \left(-\frac{\mathrm{d}J(E,\bar{p})}{\mathrm{d}E}\right) , \tag{3.53}$$

where the summation is taken over each orbital point, δt is the elapsed time between two successive orbit points, $\Delta\Omega$ the opening solid angle (`XOMEGA`), $J(E,\bar{p})$ is the `TREP` omnidirectional integral spectrum and W is the anisotropy correction factor [see Eqs. (3.32)] where the look direction (ζ,η) is related to the correct proton velocity direction (α,ϕ). The orbit-averaged

Table 3.6. Format of the file PROJECT.SPD. When more than one trajectory is specified, the whole structure is repeated.

Record	Format	Description
1	7X,I12,12X, 3I12	Number of look directions (NDIR) and starting date (year, month, day)
2	7X, <NDIR>F12.2	Polar angle (deg) for each direction (DALPH)
3	7X, <NDIR>F12.2	Azimuthal angle (deg) for each direction (DBETA)
4	7X,I12,12X, 3F12.2	Number of energies (NENERP) and location $\bar{p}$ of the satellite (altitude, latitude and longitude)
5	F7.1, <NDIR>E12.4	Energy and conversion factor $W(E, \bar{p}, \zeta, \eta)$ for each direction
⋮		⋮
4+NENERP	F7.1, <NDIR>E12.4	Energy and conversion factor for each direction
5+NENERP		Same as lines 4–$(4 +$ NENERP$)$ for the second location
⋮		⋮
–		Blank line

integral spectra are computed as

$$\overline{J}(E, \zeta, \eta) = \int_E^\infty \overline{j}(E', \zeta, \eta)\, \mathrm{d}E' \,. \tag{3.54}$$

When the namelist parameter IFULL is greater than zero, the file PROJECT.SPD is generated. This file contains the angular distribution of the trapped proton fluxes along the orbit. The format of this file is described in Table 3.6.

3.5.2.1 Program check

To test the ANISO we have calculate the right hand side of the following equality:

$$\overline{J}(E) = \sum_{\zeta,\eta} \overline{J}(E, \zeta, \eta) \tag{3.55}$$

and compared it to the orbit-averaged omnidirectional integral spectrum provided by TREP. In Fig. 3.21, the relative difference (in percentage) between the two spectra is presented as a function of the proton energy. It corresponds to fifteen consecutive orbits at 300 km perigee,

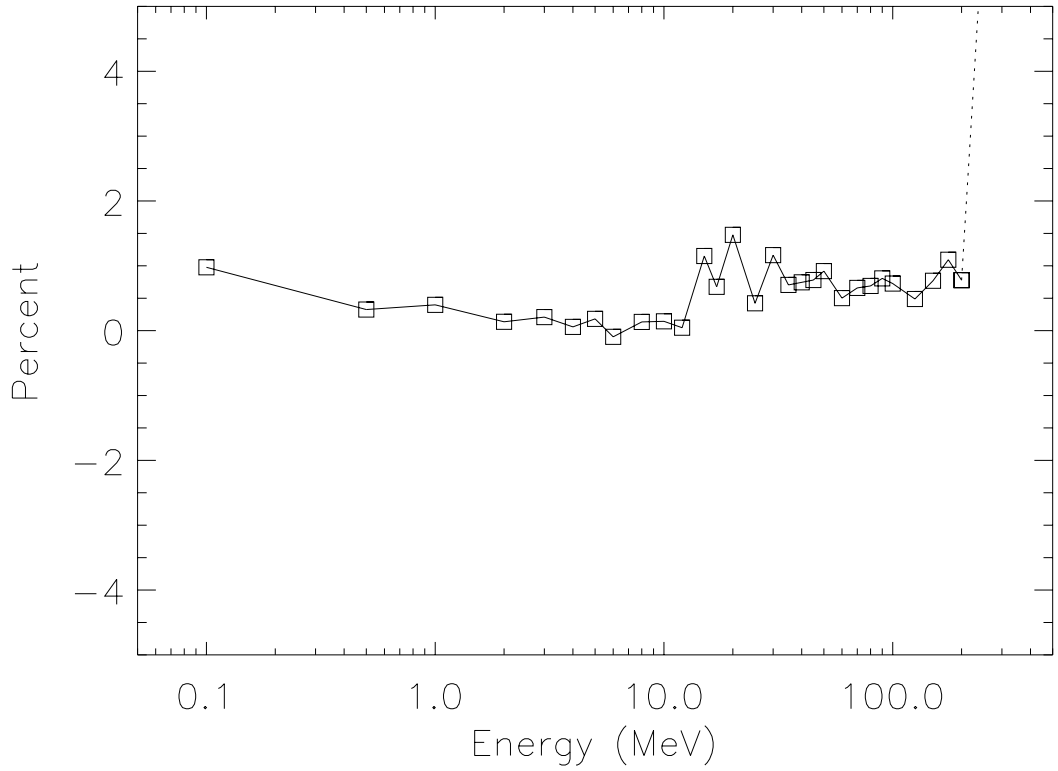

Figure 3.21. Relative difference between the orbit-averaged omnidirectional integral spectrum produced respectively by ANISO and by TREP. This average is evaluated over fifteen consecutive orbits at 300 km perigee, 2,000 km apogee and 28.5° inclination. The trapped proton models are AP-8 MIN and VF1MIN, respectively for TREP and ANISO.

2,000 km apogee and 28.5° inclination. The unidirectional flux is computed over the 180 default look directions. The omnidirectional integral spectrum provided by ANISO is almost identical to the TREP spectrum which is a test of validity of the numerical code. The very small differences are due to

1. the numerical differentiation of the TREP omnidirectional integral spectrum $J(E, \bar{p})$,
2. the approximations in the normalisation of the anisotropy factor $W(E, \bar{p}, \zeta, \eta)$,
3. the numerical integration of the orbit-averaged differential spectrum $\overline{j}(E, \zeta, \eta)$,
4. the finite size of the opening solid angle $\Delta\Omega$.

In spite of all these sources of errors, the differences remain very small. This leads us to conclude that the ANISO program is functioning correctly.

Table 3.7. Interactive menu options of ANISOPOS

Code		Action
1		Modify the title
2		Change the geomagnetic field model:
	21	– IGRF/DGRF
	22	– Jensen and Cain (1962)
	23	– GSFC 12/66
3		Modify the epoch of the geomagnetic field model
4		Change the trapped proton anisotropy model:
	41	– VF1MIN
	42	– VF1MAX
	43	– BK-MIN
	44	– BKMAX
5		Change the omnidirectional integral flux:
	51	– Power law spectrum, defined by two energies and two flux values
	52	– Exponentially decreasing spectrum, defined by two energies and two flux values
	53	– PROJECT.TRI
6		Modify the lower energy of the spectrum
7		Modify the upper energy of the spectrum
8		Specify the geodetic altitude of the point of observation
9		Specify the geodetic latitude of the point of observation
10		Specify the geographic longitude of the point of observation
11		Evaluate the (B, L) coordinates of the point of observation
0		Run the model
-1		Exit and print the results

3.5.3 ANISOPOS

As a byproduct of ANISO a standalone program called ANISOPOS has also been developed. This program evaluates the trapped proton flux anisotropy at a given single location. ANISOPOS works interactively and is self-explanatory.

The user has to supply a project name, a title, an internal geomagnetic field model [e.g. Jensen & Cain (1962)], and the geographical coordinates of a point of observation, and has to select an anisotropy model (e.g. BK-MIN or VF1MIN). The integral flux is generated either by a ASCII input file (PROJECT.TRI) or as a fit to a power law or to an exponential function. Here the user has to input two values of the particle energy corresponding to the range of energy over which the fit is performed and two value of the integral flux. ANISOPOS takes its input interactively from the keyboard. The different commands are given in Table 3.7.

ANISOPOS calculates the unidirectional differential and integral trapped proton fluxes and generates the output files PROJECT.TRD and PROJECT.TRI.

Table 3.8. ANISOPOS namelist parameters. This namelist is only used for non-interactive applications.

Parameter	Type	Default	Function
TITLE	A*56		Project header
GDALT	R*8	500	Geodetic altitude in km
GDLAT	R*8	-35°	Geodetic latitude in degrees
GDLON	R*8	300°	Geographic longitude in degrees
MODEL	I*4	0	Geomagnetic field model number, from 0 to 2
BLTIME	R*8	1995	Epoch for the geomagnetic field model IGRF
GSFCTIME	R*8	1970	Epoch for the geomagnetic field model GSFC 12/66
JANIS	I*4	1	Anisotropy model number
SPECTRUM	I*4	1	Omnidirectional integral flux number (1–3). The integral flux is defined by the file PROJECT.TRI when SPECTRUM $= 3$.
ENG01	R*8	1	When SPECTRUM is less than 3, energy of the lower limit of the spectrum, in MeV
FJ01	R*8	10^5	When SPECTRUM is less than 3, integral flux at ENG01
ENG10	R*8	10	When SPECTRUM is less than 3, energy of the upper limit of the spectrum, in MeV
FJ10	R*8	10^4	When SPECTRUM is less than 3, integral flux at ENG10

The file PROJECT.TRI contains the omnidirectional fluxes while PROJECT.TRD contains the matrix of unidirectional fluxes for a set of look angles.

For non-interactive applications, ANISOPOS takes its input from the namelist ANISOPOS of the file PROJECT.NML. The parameters of the namelist are listed in Table 3.8.

3.5.3.1 Example

A sample run of ANISOPOS is presented in Fig. 3.22. It corresponds to the angular distribution of trapped proton differential flux predicted by VF1MIN. The flux is evaluated at the 60°W, 35°S and altitude 450 km. The location and the trapped proton anisotropy model are the same as those used in Fig. 3.13. The omnidirectional flux is fixed to

$$J(E) = 10^4 \left(\frac{E}{10\,\mathrm{MeV}}\right)^{-4} \mathrm{cm}^{-2}\mathrm{s}^{-1}\,. \tag{3.56}$$

Each panel of Fig. 3.22 is the polar plot of the angular distribution in a different plane. The radius of each curve is proportional to the directional flux intensity. The different curves correspond respectively to the integral flux for proton energies above E =30, 40 and 50 MeV.

The upper left panel corresponds to the local mirror plane, i.e. the plane which is perpendicular to the magnetic field direction. The horizontal axis corresponds to the intersection between the local mirror plane and the local horizontal plane. This intersection determines the local magnetic East and West directions. The upper left panel illustrates clearly the East-West effect.

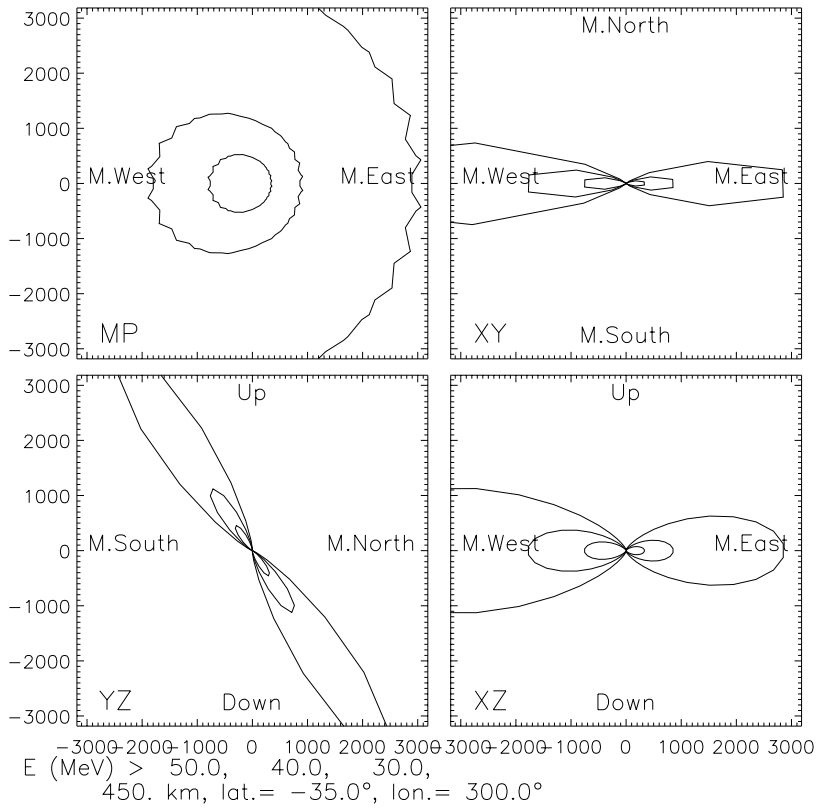

Figure 3.22. Angular distribution of trapped proton integral flux at 60°W, 35°S and altitude 450 km for 30, 40 and 50 MeV proton energies as obtained from the VF1MIN model. The upper left panel corresponds to the local mirror plane. The other three panels correspond to cut view in the planes xy, yz and xz of the satellite coordinate system in the horizontal plane. The z-axis points to the zenithal direction and the x-axis points to the East direction in the horizontal plane.

The upper right panel corresponds to a cut view in the local horizontal plane. The horizontal axis is the same as in the upper left panel. The vertical axis lies in the local horizontal plane and is perpendicular to the local magnetic East-West axis: it determines the local magnetic North and South direction. At the point of observation, the loss cone occupies a large fraction of the solid angle.

The lower left and lower right panels correspond to cut views in two vertical planes. At the point of observation, the magnetic field line is parallel to the plane of the lower left panel. The horizontal axis in this panel corresponds to the local magnetic North-South axis. The pitch-angle distribution is nicely illustrated in this panel.

The lower right panel corresponds to the plane perpendicular to the one of the lower left panel. Its horizontal axis corresponds to the magnetic East-West axis. These four panels provide to the user a reliable sketch of the trapped proton anisotropy at the point of observation.